

Type-X two Higgs doublet model in light of the muon $g - 2$: confronting Higgs and collider data

Adil Jueid,^{1,*} Jinheung Kim,^{1,†} Soojin Lee,^{1,‡} and Jeonghyeon Song^{1,§}

¹*Department of Physics, Konkuk University, Seoul 05029, Republic of Korea*

Abstract

The recent Fermilab measurement of the muon anomalous magnetic moment yields 4.2σ deviations from the SM prediction when combined with the BNL E821 experiment results. In the Type-X two Higgs doublet model, we study the consequence of imposing the observed muon $g - 2$, along with the constraints from theoretical stabilities, electroweak oblique parameters, Higgs precision data, and direct searches. For a comprehensive study, we scan the whole parameter space in two scenarios, the normal scenario where $h_{\text{SM}} = h$ and the inverted scenario where $h_{\text{SM}} = H$, where h (H) is the light (heavy) CP -even Higgs boson. We found that large $\tan \beta$ (above 100) and light pseudoscalar mass M_A are required to explain the muon $g - 2$ anomaly. This breaks the theoretical stability unless the scalar masses satisfy $M_A^2 \simeq M_{H^\pm}^2 \simeq m_{12}^2 \tan \beta \approx M_{H/h}^2$. The direct search bounds at the LEP and LHC exclude the light A window with $M_A \lesssim 62.5$ GeV. We also show that the observed electron anomalous magnetic moment is consistent with the model prediction, but the lepton flavor universality data in the τ and Z decays are not. For a separate exploration of the model, we propose the golden mode $pp \rightarrow Ah/AH \rightarrow 4\tau$ at the HL-LHC.

PACS numbers:

*Electronic address: adiljueid@konkuk.ac.kr

†Electronic address: jinheung.kim1216@gmail.com

‡Electronic address: soojinlee957@gmail.com

§Electronic address: jhsong@konkuk.ac.kr

Contents

I. Introduction	2
II. Type-X 2HDM	4
III. Δa_μ in the Type-X 2HDM	6
IV. Theoretical and experimental constraints on the Type-X 2HDM	8
A. Scanning strategies in three steps	8
B. Results in the normal scenario	9
C. Results in the inverted scenario	11
V. Implications on the electron $g - 2$ and the LHC collider signatures	13
A. Electron anomalous magnetic moment	14
B. Production of the hadro-phobic new scalars at the LHC	14
VI. Lepton flavor universality data in the τ and Z decays	18
VII. Conclusion	21
Acknowledgments	22
A. Used parameters in the τ^\pm and Z decays for the global χ^2 analysis	22
References	23

I. INTRODUCTION

The recent measurement of the muon anomalous magnetic moment by the Fermilab National Accelerator Laboratory (FNAL) Muon $g - 2$ experiment [1, 2] achieved unprecedented precision. When combined with the old result of the Brookhaven National Laboratory (BNL) E821 measurement [3], it reads as

$$a_\mu^{\text{exp}} = 116\,592\,061(41) \times 10^{-11}, \quad (1)$$

where $a_\mu = (g - 2)_\mu/2$. As the experimental error is becoming comparable with the theoretical error,¹ reliable and accurate calculation of the SM prediction is more important than ever. The recent progress includes five loops in QED [4] and two loops in electroweak interactions [5, 6]. Nevertheless, the most dominant contribution is from the strong interaction dynamics at $\mathcal{O}(1)$ GeV, which is categorized into the hadronic vacuum polarization (HVP) [7–14] and the

¹ The experimental measurement will be improved in a short time scale. For instance, FNAL will provide a new measurement of a_μ in the summer of 2022 after including more datasets.

hadronic light-by-light (HLbL) scattering [15–27]. These QCD corrections cannot be computed using perturbation theory. We have to resort to non-perturbative methods, either Lattice QCD or data-driven methods. On the Lattice side, the recent calculation of the leading order HVP (LO-HVP) contributions to a_μ by the Budapest-Marseille-Wuppertal collaboration [28] yields $a_\mu|_{\text{LO-HVP}} = 707.5(5.3) \times 10^{-10}$. If we take this result at face value, the Fermilab measurement of a_μ is consistent with the SM prediction at $\sim 2\sigma$. On the data-driven method side, however, the calculation of the HVP contribution [9, 11, 12] supports the long-standing discrepancy between the muon $g - 2$ experiment and the SM prediction, as

$$\Delta a_\mu^{\text{obs}} = a_\mu^{\text{exp}} - a_\mu^{\text{SM}} = 251(59) \times 10^{-11}. \quad (2)$$

Which method is more appropriate needs further investigation. One checking point is the connection of the QCD corrections to electroweak precision fits [29–32], since some of the most important inputs to HVP and HLbL contributions come from measuring the $R(s)$ -ratio in e^+e^- collisions. Lately, some tension was reported between the Lattice result and the electroweak data [30, 31]. Another critical topic is how to combine the probability distribution functions with different errors.

In this paper, we take the 4.2σ deviation in Eq. (2), which calls for new physics (NP) explanation. In a short time, various NP models have been vigorously studied for the muon $g-2$, focusing on a supersymmetric theory [33–45], leptophilic boson model [46, 47], singlet scalar model [48], three Higgs doublet model [49], leptoquark model [50, 51], $L_\mu - L_\tau$ model [52, 53], $B - L$ or $B - 3L$ gauge model [54, 55], flavorful scalar model [56], seesaw model [57], simplified model with minimal field contents [58], effective field theory [59], axion model [60, 61], two Higgs doublet model (2HDM) [62–71], or 2HDM with a singlet scalar model [72, 73]. These efforts shall continue because each NP model as a solution for the observed Δa_μ should simultaneously explain a vast amount of experimental data in particle physics.

From this motivation, we study the CP invariant Type-X (lepton-specific) 2HDM in light of the muon $g-2$. In Type-X, the couplings of the new scalar bosons to the SM quarks are inversely proportional to $\tan\beta$, the ratio of two vacuum expectation values of two Higgs doublet fields, but those to the charged leptons are linearly proportional to $\tan\beta$. Large $\tan\beta$ can enhance the new contributions of extra Higgs bosons to Δa_μ , while suppressing the contributions to the hadron-related data such as $B \rightarrow K\mu^+\mu^-$ and $B_s \rightarrow \mu^+\mu^-$ [74]. Since the other three types (Type-I, Type-II, and Type-Y) cannot accommodate this feature, there have been extensive studies of Type-X for the muon anomalous magnetic moment [75–82].

A comprehensive study of Type-X for Δa_μ , including the LHC Run-1 and LEP results as well as the lepton flavor universality (LFU) data in the Z and τ decays, was first conducted in Ref. [78]. Partial updates have followed, focusing on the LFU data [79] or the LHC data [80–82]. We generalize the previous studies of the Type-X 2HDM both in theoretical setup and in data analysis. First, we take the general setting in the Higgs sector, by considering two scenarios, the “normal” scenario where the observed Higgs boson is the lighter CP -even scalar h and the “inverted” scenario where the heavier CP -even scalar H is the observed one. The

inverted scenario with a new light CP -even scalar has recently drawn a lot of interest because of the 3σ excess in the diphoton invariant mass distribution at around 96 GeV [83], but has not been analyzed in the context of the muon $g - 2$. This scenario seems incompatible with the recent measurement of *positive* Δa_μ , because the dominant Barr-Zee contributions of the τ^\pm loop mediated by the light CP -even h are *negative* [84, 85]. We need to answer whether the inverted scenario remains viable.

For the general data analysis, we will investigate all the latest data of the LHC Run-2, the electron anomalous magnetic moment [86, 87], the LFU data (adopting the updated HFLAV global fit results [88] and Michel parameters [89] in the τ decay), as well as theoretical stabilities and electroweak oblique parameters. We will also include the correlations among the observables. The correlations are often neglected in the literature, but they play a vital role in constraining new physics models. To draw a general conclusion on the Type-X 2HDM, we will scan the whole parameter space without any extra assumption on the masses or the couplings. Furthermore, the tension in the Type-X when simultaneously explaining Δa_μ and LFU data shall be quantified through the global χ^2 fit. Finally, the customized search strategy for the viable parameter space at the HL-LHC is to be studied. These are our contributions to the phenomenology of the Type-X 2HDM in light of the new Fermilab measurement of Δa_μ .

The paper is organized in the following way. In Sec. II, we briefly review the Type-X 2HDM and describe the characteristics of the normal and inverted scenarios in the Higgs alignment limit. In Sec. III, we discuss the new contributions of the Type-X 2HDM to Δa_μ . Section IV describes our scanning strategies in three steps and shows the results of the allowed parameter space at each step. Section V deals with the electron anomalous magnetic moment and the LHC signatures. In Sec. VI, we check the consistency of the model with the LFU data in the τ and Z decays. Conclusions are given in Sec. VII.

II. TYPE-X 2HDM

The 2HDM accommodates two complex $SU(2)_L$ Higgs doublet scalar fields, Φ_1 and Φ_2 [90]:

$$\Phi_i = \begin{pmatrix} w_i^+ \\ \frac{v_i + h_i + i\eta_i}{\sqrt{2}} \end{pmatrix}, \quad i = 1, 2, \quad (3)$$

where $v = \sqrt{v_1^2 + v_2^2} = 246$ GeV. Using the simplified notation of $s_x = \sin x$, $c_x = \cos x$, and $t_x = \tan x$, we define $t_\beta = v_2/v_1$. To prevent the tree-level flavor changing neutral currents, a discrete Z_2 symmetry is imposed as $\Phi_1 \rightarrow \Phi_1$ and $\Phi_2 \rightarrow -\Phi_2$ [91, 92]. The most general, renormalizable, and CP conserving scalar potential with softly broken Z_2 symmetry is

$$\begin{aligned} V_\Phi = & m_{11}^2 \Phi_1^\dagger \Phi_1 + m_{22}^2 \Phi_2^\dagger \Phi_2 - m_{12}^2 (\Phi_1^\dagger \Phi_2 + \text{H.c.}) \\ & + \frac{1}{2} \lambda_1 (\Phi_1^\dagger \Phi_1)^2 + \frac{1}{2} \lambda_2 (\Phi_2^\dagger \Phi_2)^2 + \lambda_3 (\Phi_1^\dagger \Phi_1) (\Phi_2^\dagger \Phi_2) + \lambda_4 (\Phi_1^\dagger \Phi_2) (\Phi_2^\dagger \Phi_1) \\ & + \frac{1}{2} \lambda_5 [(\Phi_1^\dagger \Phi_2)^2 + \text{H.c.}], \end{aligned} \quad (4)$$

where the m_{12}^2 term softly breaks the Z_2 parity. There are five physical Higgs bosons, the light CP -even scalar h , the heavy CP -even scalar H , the CP -odd pseudoscalar A , and two charged Higgs bosons H^\pm . The relations of the physical Higgs bosons with the weak eigenstates in Eq. (3) via two mixing angles α and β are referred to Ref. [93, 94]. Note that the SM Higgs boson is a linear combination of h and H , as

$$h_{\text{SM}} = s_{\beta-\alpha}h + c_{\beta-\alpha}H. \quad (5)$$

The Yukawa couplings to the SM fermions are written by

$$\begin{aligned} \mathcal{L}_{\text{Yuk}} = & - \sum_f \left(\frac{m_f}{v} y_f^h \bar{f} f h + \frac{m_f}{v} y_f^H \bar{f} f H - i \frac{m_f}{v} y_f^A \bar{f} \gamma_5 f A \right) \\ & - \left\{ \frac{\sqrt{2}}{v} \bar{t} (m_t y_t^A P_L + m_b y_b^A P_R) b H^+ + \frac{\sqrt{2} m_\ell}{v} y_\ell^A \bar{\nu}_\ell P_R \ell H^+ + \text{H.c.} \right\}, \end{aligned} \quad (6)$$

where $P_{R,L} = (1 \pm \gamma^5)/2$ and $\ell = \mu, \tau$.

The observed Higgs boson at a mass of 125 GeV is similar to the SM Higgs boson, more strongly in Type-X with large t_β [95]. Therefore, we take the Higgs alignment limit where one of the CP -even neutral Higgs bosons is the SM Higgs boson h_{SM} [96–100]. There are two ways to realize the Higgs alignment limit, the “normal” and “inverted” scenarios. In the normal scenario, the observed Higgs boson is the lighter CP -even scalar h , i.e., $s_{\beta-\alpha} = 1$. In the inverted scenario, $c_{\beta-\alpha} = 1$ so that the heavier CP -even scalar H is observed while the lighter one is hidden [99, 101]. The model has five independent parameters in the physical basis,

$$\{m_{\varphi^0}, M_A, M_{H^\pm}, M^2, t_\beta\}, \quad (7)$$

where $M^2 = m_{12}^2/(s_\beta c_\beta)$ and φ^0 is the new CP -even neutral Higgs boson, i.e., $\varphi^0 = H$ in the normal scenario and $\varphi^0 = h$ in the inverted scenario. The two scenarios are summarized as follows:

normal scenario (NS)	inverted scenario (IS)
$h_{\text{SM}} = h, \quad \varphi^0 = H$	$h_{\text{SM}} = H, \quad \varphi^0 = h$
$y_f^{h_{\text{SM}}} = 1, \quad s_{\beta-\alpha} = 1$	$y_f^{h_{\text{SM}}} = 1, \quad c_{\beta-\alpha} = 1$
$y_t^A = -y_t^{\varphi^0} = \frac{1}{t_\beta}, \quad y_\ell^A = y_\ell^{\varphi^0} = t_\beta$	$y_t^A = y_t^{\varphi^0} = \frac{1}{t_\beta}, \quad y_\ell^A = -y_\ell^{\varphi^0} = t_\beta$

(8)

In the Higgs alignment limit, the quartic couplings are [100]

$$\begin{aligned}
\lambda_1 &= \frac{1}{v^2} [m_{125}^2 + t_\beta^2 (m_{\varphi^0}^2 - M^2)], \\
\lambda_2 &= \frac{1}{v^2} \left[m_{125}^2 + \frac{1}{t_\beta^2} (m_{\varphi^0}^2 - M^2) \right], \\
\lambda_3 &= \frac{1}{v^2} [m_{125}^2 - m_{\varphi^0}^2 - M^2 + 2M_{H^\pm}^2], \\
\lambda_4 &= \frac{1}{v^2} [M^2 + M_A^2 - 2M_{H^\pm}^2], \\
\lambda_5 &= \frac{1}{v^2} [M^2 - M_A^2],
\end{aligned} \tag{9}$$

where $m_{125} = 125$ GeV. As shall be shown in the next section, the observed Δa_μ requires large t_β . Then, the t_β^2 terms in λ_1 easily break the perturbativity of λ_1 unless $m_{\varphi^0}^2$ is extremely close to M^2 , which is to be denoted by $m_{\varphi^0}^2 \approx M^2$. When applying this approximate equality to the perturbativity of λ_3 , we should accommodate quasi-degeneracy between M^2 and $M_{H^\pm}^2$. The mass degeneracy is weaker because of the absence of t_β^2 terms in λ_3 . We use the notation of $M^2 \simeq M_{H^\pm}^2$ for the weak equality. The perturbativity of λ_4 and λ_5 finally yields $M_A \simeq M_{H^\pm}$. In summary, the perturbativity of the quartic couplings for large t_β limits the masses as

$$M_A \simeq M_{H^\pm} \simeq M \approx m_{\varphi^0}. \tag{10}$$

For light M_A , the exotic Higgs decay of $h_{\text{SM}} \rightarrow AA$ severely restricts the model. When writing $\mathcal{L} = (1/2)\lambda_{AA}^{h_{\text{SM}}} h_{\text{SM}} AA$, the vertex is

$$\lambda_{AA}^{h_{\text{SM}}} = \frac{1}{v} (-m_{125}^2 - 2M_A^2 + 2M^2). \tag{11}$$

Because of the condition in Eq. (10), it is difficult to accommodate $\lambda_{AA}^{h_{\text{SM}}} = 0$.² Since the Higgs precision measurement puts a strong bound on the exotic Higgs decay as $\mathcal{B}(h_{\text{SM}} \rightarrow XX) \lesssim \mathcal{O}(0.1)$ [102], the parameter region with $M_A \leq m_{125}/2$ is highly disfavored.

III. Δa_μ IN THE TYPE-X 2HDM

The Type-X 2HDM makes two kinds of new contributions to Δa_μ , one-loop contributions and two-loop Barr-Zee contributions [84, 85]. The one-loop contributions are mediated by φ^0 , A , and H^\pm , as [80]

$$\begin{aligned}
\Delta a_\mu^{1\text{-loop}} &= \frac{G_F m_\mu^2}{4\pi^2 \sqrt{2}} \sum_\phi (y_\mu^\phi)^2 \rho_\phi^\mu f_\phi(\rho_\phi^\mu) \\
&\simeq 2.6 \times 10^{-15} \sum_\phi (y_\mu^\phi)^2 \left(\frac{100 \text{ GeV}}{M_\phi} \right)^2 f_\phi(\rho_\phi^\mu),
\end{aligned} \tag{12}$$

² If the Higgs alignment is broken and $t_{\beta-\alpha} = (t_\beta - 1/t_\beta)(M^2 - m_{125}^2)/(2M^2 - 2M_A^2 - m_{125}^2)$, $\lambda_{AA}^{h_{\text{SM}}}$ vanishes and the constraint from $h_{\text{SM}} \rightarrow AA$ can be evaded. However, the equality involves five independent parameters of α , β , m_{125} , M^2 , and M_A , which is an unnatural fine-tuning without underlying symmetries.

where $\phi = \{\varphi^0, A, H^\pm\}$, $\rho_j^i = m_i^2/m_j^2$, and the expressions for the loop function f_ϕ are referred to Ref. [80]. The numerical factor in the second equality of Eq. (12) implies that the observed Δa_μ requires light M_ϕ and large y_μ^ϕ . Because $\rho_\phi^\mu \ll 1$, the loop functions show the following asymptotic behaviors:

$$\begin{aligned} f_{\varphi^0}(\rho) &= -\ln \rho - 7/6 + \mathcal{O}(\rho), \\ f_A(\rho) &= +\ln \rho + 11/6 + \mathcal{O}(\rho), \\ f_{H^\pm}(\rho) &= -1/6 + \mathcal{O}(\rho). \end{aligned} \quad (13)$$

It is clear to see that the one-loop contributions of the CP -even scalar φ^0 are positive while those of A and H^\pm are negative: $\Delta a_\mu^{1\text{-loop}}$ is proportional to the *square* of y_μ^ϕ .

More significant contributions to Δa_μ are from the two-loop Barr-Zee type diagrams with heavy fermions in the loop [84]:

$$\Delta a_\mu^{\text{BZ}} = \frac{G_F m_\mu^2}{4\pi^2 \sqrt{2}} \frac{\alpha_{\text{em}}}{\pi} \sum_{f, \phi^0} N_f^c Q_f^2 y_\mu^{\phi^0} y_f^{\phi^0} \rho_{\phi^0}^f g_{\phi^0}(\rho_{\phi^0}^f), \quad (14)$$

where $f = t, b, \tau$, $\phi^0 = \{\varphi^0, A\}$, m_f , Q_f and N_f^c are the mass, electric charge and color factor of the fermion f , and the loop functions are

$$\begin{aligned} g_{\varphi^0}(\rho) &= \int_0^1 dx \frac{2x(1-x) - 1}{x(1-x) - \rho} \ln \frac{x(1-x)}{\rho}, \\ g_A(\rho) &= \int_0^1 dx \frac{1}{x(1-x) - \rho} \ln \frac{x(1-x)}{\rho}. \end{aligned} \quad (15)$$

For the top quark and τ^\pm loops, the factor $\rho_{\phi^0}^f$ in Eq. (14) significantly enhances Δa_μ^{BZ} with respect to $\Delta a_\mu^{1\text{-loop}}$ in Eq. (12). The usual conclusion that a CP -even scalar boson makes a negative contribution to Δa_μ^{BZ} holds true when $y_\mu^{\varphi^0} y_f^{\varphi^0} > 0$. As shown in Eq. (8), the top quark incorporates $y_\mu^{\varphi^0} y_t^{\varphi^0} < 0$ in both scenarios and thus generates *positive* two-loop Barr-Zee contributions.

In Fig. 1, we show $\Delta a_\mu(A)$ (blue line), $-\Delta a_\mu(\varphi^0)$ (red line), and $\Delta a_\mu(A) + \Delta a_\mu(\varphi^0)$ (black line) as a function of t_β with $M_A = m_{\varphi^0} = 100$ GeV in the left panel and as a function of $M_A = m_{\varphi^0}$ with $t_\beta = 100$ in the right panel. To show negative $\Delta a_\mu(\varphi^0)$ in the logarithmic scale, we present $-\Delta a_\mu(\varphi^0)$. The horizontal green (yellow) area denotes the allowed region of Δa_μ at 1σ (2σ). The dominant contribution of A is from two-loop Barr-Zee diagrams, which is always positive. The sign of the φ^0 contribution depends on the value of t_β . For very large t_β , $\Delta a_\mu(\varphi^0)$ is negative since the contribution of the τ^\pm loop in the two-loop Barr-Zee diagram is dominant. If $t_\beta \lesssim 17$, however, $\Delta a_\mu(\varphi^0)$ becomes positive (see the small figure inside the left panel) because dominant is the top quark loop in the two-loop Barr-Zee diagram. Although the contributions from both A and φ^0 are positive for $t_\beta \lesssim 17$, the absolute value of Δa_μ is not large enough to explain $\Delta a_\mu^{\text{obs}}$. In the right panel, we show $\Delta a_\mu(A)$ and $-\Delta a_\mu(\varphi^0)$ as a function of $M_A = m_{\varphi^0}$ by fixing $t_\beta = 100$. Δa_μ increases rapidly with decreasing scalar masses. Since the negative contributions of the CP -even φ^0 become severe with decreasing m_{φ^0} , the inverted scenario receives a stronger constraint.

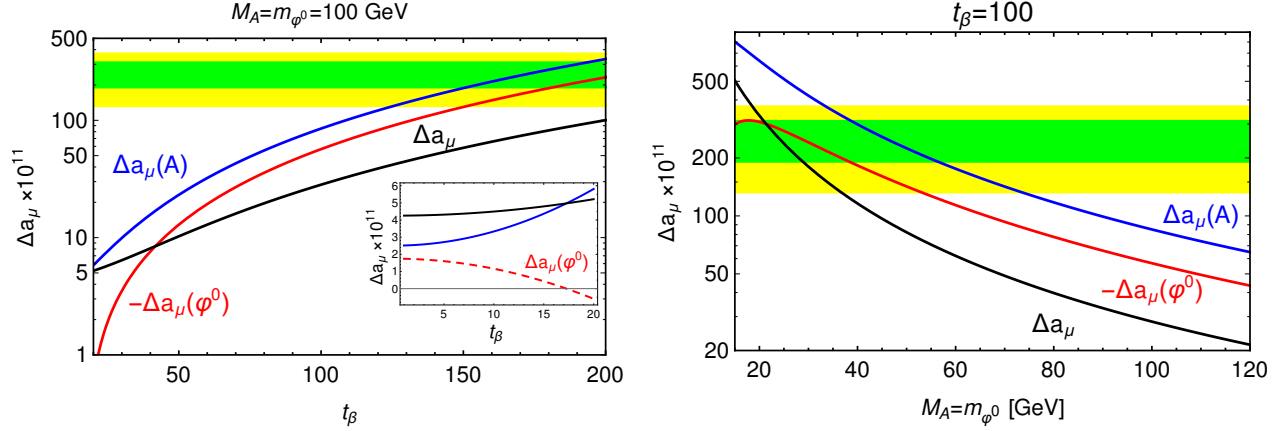


FIG. 1: Δa_μ from A , $-\Delta a_\mu$ from φ^0 , and $\Delta a_\mu(A) + \Delta a_\mu(\varphi^0)$ as a function of t_β with $M_A = m_{\varphi^0} = 100 \text{ GeV}$ (left panel) and as a function of $M_A = m_{\varphi^0}$ for $t_\beta = 100$ (right panel).

IV. THEORETICAL AND EXPERIMENTAL CONSTRAINTS ON THE TYPE-X 2HDM

A. Scanning strategies in three steps

For the comprehensive study of the Type-X 2HDM in light of the muon $g - 2$, we perform the successive and cumulative scan of the model parameters in three steps.

Step I: We demand that the model explains $\Delta a_\mu^{\text{obs}}$ at 2σ .

Step II: Among the parameters that survive Step I, we impose the constraints from theoretical stabilities and electroweak precision data, as detailed below.

1. Theoretical stabilities [99, 103, 104]
 - Higgs potential being bounded from below [103];
 - Unitarity of scalar-scalar scatterings [90, 105];
 - Perturbativity [99];
 - Vacuum stability [104].

2. Peskin-Takeuchi electroweak oblique parameters [106]

We take the current best-fit results of [107]

$$\begin{aligned}
S &= -0.01 \pm 0.10, & T &= 0.03 \pm 0.12, & U &= 0.02 \pm 0.11, \\
\rho_{ST} &= 0.92, & \rho_{SU} &= -0.80, & \rho_{TU} &= -0.93,
\end{aligned} \tag{16}$$

where ρ_{ij} is the correlation matrix. The expressions of the contributions from the scalar boson loops to S , T , and U are referred to Ref. [108, 109]. We require $\Delta\chi^2 (= \chi^2 - \chi_{\text{min}}^2) < 7.81$.

Step III: For the parameters that survive Step II, we demand to satisfy the collider bounds.

1. Higgs precision data by using `HiggsSignals` [110, 111]:
The `HiggsSignals-v2.2.0` [111] provides the χ^2 value for 107 Higgs observables. Since our model has five parameters, the number of degrees of freedom for the χ^2 analysis is 102. We require that the calculated Higgs signal strengths be consistent with the experimental measurements at 2σ .
2. Direct searches for new scalars at the LEP, Tevatron, and LHC:
We use the public code `HiggsBounds` [112]. Main search channels which affect the Type-X 2HDM are
 - (a) LEP experiments:
 - $e^+e^- \rightarrow Z \rightarrow Ah \rightarrow \tau^+\tau^-\tau^+\tau^-$ [113].
 - (b) LHC experiments:
 - $h \rightarrow AA$ [114–119];
 - $H \rightarrow ZZ/W^+W^-$ [120–122];
 - $H \rightarrow hh$ [120, 123–129];
 - $H/A \rightarrow \gamma\gamma$ [130, 131], $\tau^+\tau^-$ [132, 133], $\mu^+\mu^-$ [134–136], $b\bar{b}$ [137–139], $t\bar{t}$ [140];
 - $A \rightarrow Zh$ [141, 142];
 - $A(H) \rightarrow ZH(A)$ [143, 144];
 - $H^\pm \rightarrow tb$ [145, 146], $\tau^\pm\nu$ [147, 148].

For each scattering process, we compute the $r_{95\%}$ defined by

$$r_{95\%} = \frac{S_{\text{2HDM}}}{S_{\text{obs}}^{95\%}}, \quad (17)$$

where S_{2HDM} ($S_{\text{obs}}^{95\%}$) is the predicted (observed) cross section. A point in the parameter space is excluded at the 95% confidence level if $r_{95\%} > 1$.

In the normal scenario, we obtained 5×10^5 parameter sets that satisfy Step II. Step III excludes about 80% of the parameter sets that survived Step II. The exclusion is more severe in the inverted scenario, for which we separately collected 5×10^5 parameter sets that pass Step II. Only $\sim 1.8\%$ parameter sets survive at Step III.

B. Results in the normal scenario

In Fig. 2, we show the allowed (M_A, t_β) at each step. The observed Δa_μ at Step I (left panel) demands $t_\beta \gtrsim 30$ and $M_A \lesssim 200$ GeV, but does not limit the masses of H and H^\pm . Both M_H and M_{H^\pm} can reach about 1 TeV. At Step II (middle panel), a large cut on the parameter space is made, mainly on M_H and M_{H^\pm} . It is because the combination of the theoretical stability condition ($M_A \simeq M_{H^\pm} \simeq M_H \approx M$) and the intermediate M_A at Step I lowers M_H

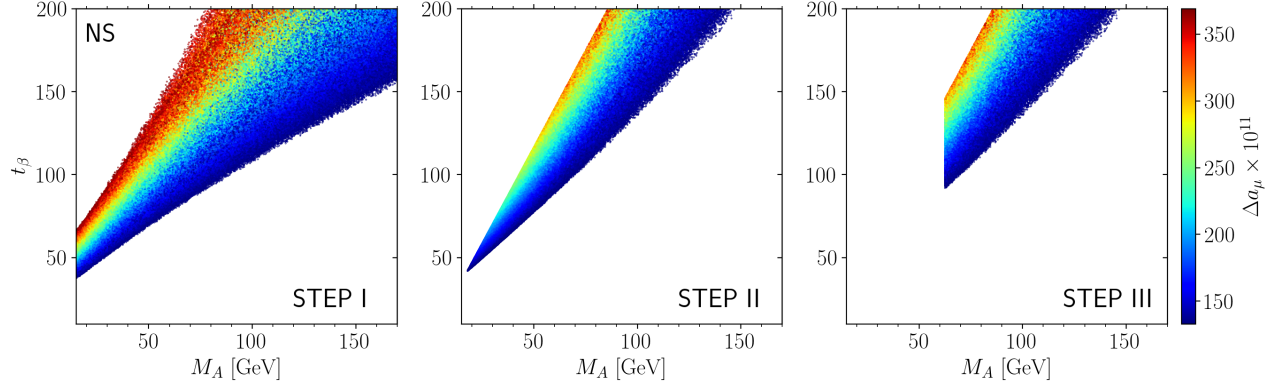


FIG. 2: In the normal scenario, the allowed parameter space of (M_A, t_β) after Step I ($\Delta a_\mu^{\text{obs}}$), Step II (Step I+Theory+EWPD), and Step III (Step II+Collider), with the color code indicating the value of Δa_μ .

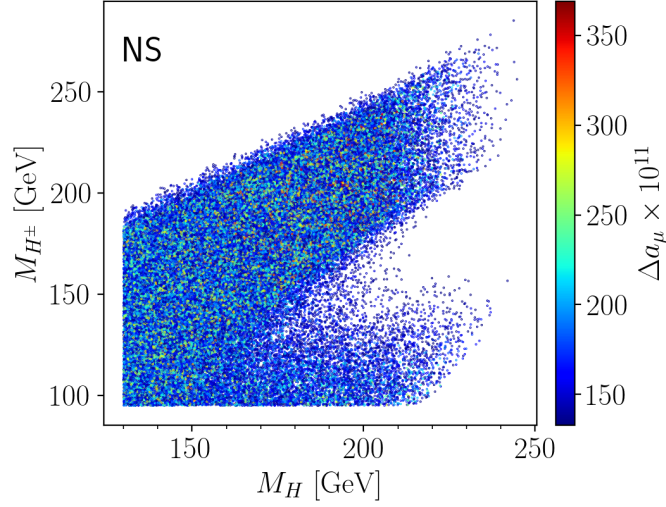


FIG. 3: The allowed (M_H, M_{H^\pm}) in the normal scenario at Step III. The color code indicates the value of Δa_μ .

and M_{H^\pm} . This feature is shown in Fig. 3 by the allowed (M_H, M_{H^\pm}) at Step III: Step II and Step III have similar results for M_H and M_{H^\pm} . There exist upper bounds of $M_H \lesssim 245$ GeV and $M_{H^\pm} \lesssim 285$ GeV. Besides, the correlation of Δa_μ with M_H or M_{H^\pm} is weak, as indicated by the mixed colors of Δa_μ . As only the intermediate M_H survives, the negative contribution of the CP -even H to Δa_μ becomes significant.

Let us go back to discussing the allowed (M_A, t_β) . At Step III, which additionally imposes the constraints from the collider data at the LEP, Tevatron, and LHC, a large portion of the parameter space is removed: see the right panel in Fig. 2. We found that the *recent* LHC

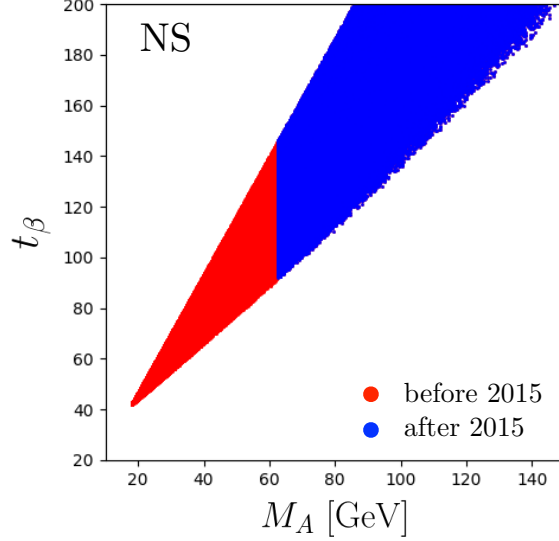


FIG. 4: In the normal scenario, the comparison of the allowed (M_A, t_β) by using the LHC data before 2015 (red) and after 2015 (blue).

data plays a crucial role in the curtailment. To demonstrate the role, we present the allowed parameter points in (M_A, t_β) by the LHC data before 2015 (red) and those after 2015 (blue) in Fig. 4: 2015 is taken as the reference point in consideration of Ref. [78]. The new LHC data exclude the whole parameter space of $M_A < m_{125}/2$ and $t_\beta \lesssim 90$. The accumulation of the LHC null results in the NP searches gives a significant implication on the Type-X 2HDM in the context of muon $g - 2$.

The question that follows is which LHC processes exclude the region of $M_A < m_{125}/2$. In principle, multiple processes exclude one parameter set simultaneously. For efficient illustration, we present in Fig. 5 the smoking-gun process that has the largest deviation of the model prediction from the observation, $r_{95\%}$ in Eq. (17). The green points pass all the constraints. The orange points are rejected by the LHC bounds on $h_{\text{SM}} \rightarrow AA \rightarrow \mu^+ \mu^- \tau^+ \tau^-$ [116, 149]. The red points are excluded by the combined LEP results of $e^+ e^- \rightarrow H^+ H^-$ including the decays of $H^+ H^-$ into $c\bar{s}c\bar{s}$, $c\bar{s}\tau\nu$, $\tau\nu\tau\nu$, $W^* A \tau\nu$, and $W^* A W^* A$ [150]. The overlap of the allowed (green) and excluded (red) points is attributed to the projection of the five-dimensional hypervolume onto the two-dimensional (M_A, t_β) plane. In summary, the normal scenario of the Type-X 2HDM in light of the muon $g - 2$ is phenomenologically viable for $t_\beta \gtrsim 90$, $M_A \in [62.5, 145]$ GeV, $M_H \in [130, 245]$ GeV, and $M_{H^\pm} \in [95, 285]$ GeV.

C. Results in the inverted scenario

In the inverted scenario, the pattern of the exclusion at Step I, Step II, and Step III is similar to that in the normal scenario: see Fig. 6. In the quantitative aspect, however, there are some differences. At Step I, the observed Δa_μ prefers lighter M_A than in the normal scenario,

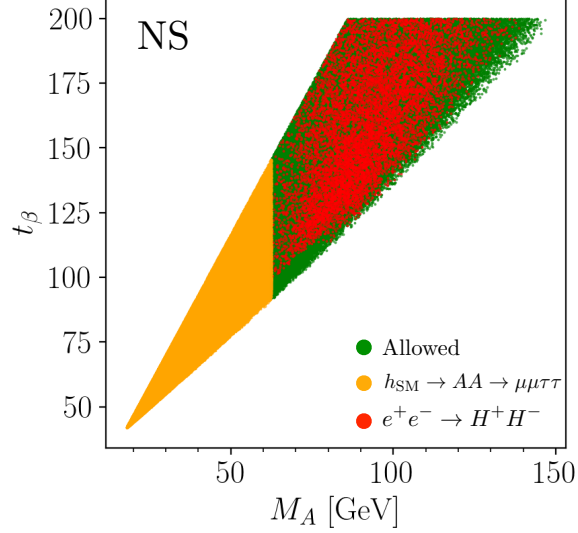


FIG. 5: In the normal scenario at Step III, the allowed points (green) and the excluded points (orange and red) in the parameter space of (M_A, t_β) . The orange points are excluded by $h_{\text{SM}} \rightarrow AA \rightarrow \mu\mu\tau\tau$ at the LHC, and the red points are excluded by $e^+e^- \rightarrow H^+H^-$ at the LEP.

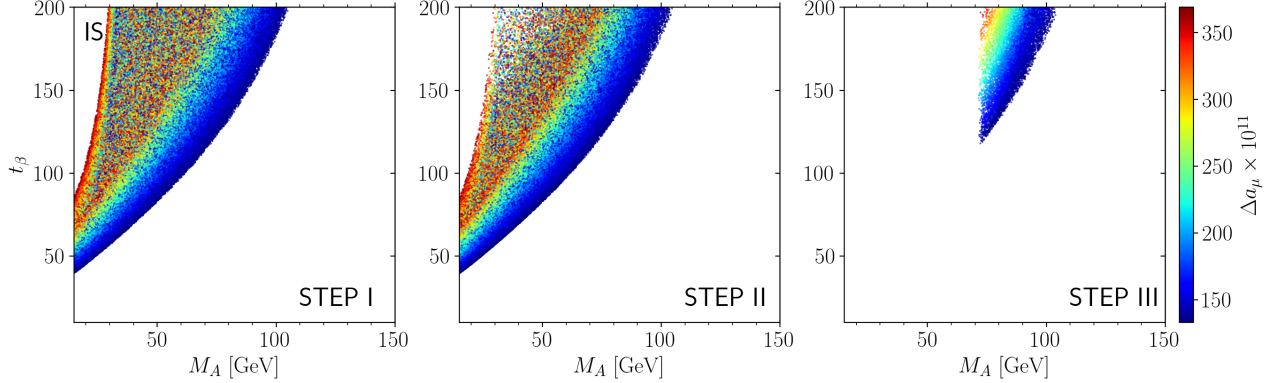


FIG. 6: In the inverted scenario, the allowed parameter space of (M_A, t_β) at Step I, Step II, and Step III, with the color code indicating the value of Δa_μ .

as the light CP -even h makes a sizably negative contribution. The constraints at Step II are weaker than in the normal scenario. The perturbativity of λ_1 , the most critical factor for the theoretical stability, is easier to satisfy with light m_h . At Step III (right panel), the collider constraints in the inverted scenario are stronger than in the normal scenario, leading to larger t_β as $t_\beta \gtrsim 120$.

Figure 7 presents the collider smoking-gun processes in the inverted scenario. The green points are finally allowed. The orange and red points are excluded by $h_{\text{SM}} \rightarrow AA$ [116, 149] and the LEP process $e^+e^- \rightarrow H^+H^-$ [150], respectively. But the most vital role is played by the LEP process $e^+e^- \rightarrow Z^* \rightarrow Ah$ [113] (blue points) because the Z - A - h vertex, proportional to

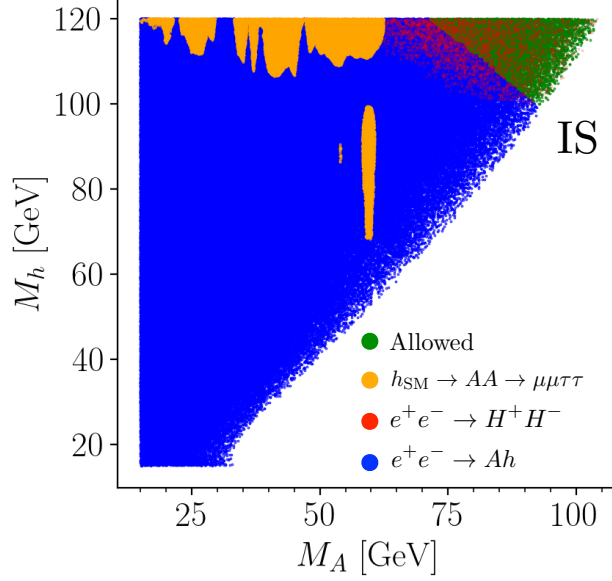


FIG. 7: In the inverted scenario at the final Step III, the allowed points (green) and the excluded points (orange, red, and blue). The orange points are excluded by $h_{\text{SM}} \rightarrow AA \rightarrow \mu^+\mu^-\tau^+\tau^-$ at the LHC, the red points by $e^+e^- \rightarrow H^+H^-$ at the LEP, and the blue points by $e^+e^- \rightarrow Ah$ at the LEP.

$c_{\beta-\alpha}$, is maximal in the alignment limit of the inverted scenario. We found that the constraint from $e^+e^- \rightarrow Ah$ is so strong that only the kinematic ban of $\sqrt{s_{ee}} < M_A + M_h$ saves the parameter point.

In Fig. 8, we present the finally allowed (M_h, M_{H^\pm}) in the inverted scenario with the color code indicating the value of Δa_μ . As in the normal scenario, there is no correlation of Δa_μ with M_h or M_{H^\pm} : see the mixed color distribution. In summary, the inverted scenario survives for $t_\beta \gtrsim 120$, $M_A \in [70, 105]$ GeV, $M_H \in [100, 120]$ GeV, and $M_{H^\pm} \in [95, 185]$ GeV.

V. IMPLICATIONS ON THE ELECTRON $g - 2$ AND THE LHC COLLIDER SIGNATURES

Upon obtaining the finally allowed parameter points of the Type-X 2HDM in light of the new muon $g - 2$, we investigate the phenomenological implications of the surviving parameters. First, we study the electron anomalous magnetic moment. For Δa_e , there is controversy over the value of the fine structure constant α . Therefore, we check the consistency of the surviving parameters with Δa_e rather than accept Δa_e as an observable. Second, we study the LHC phenomenology so to suggest the golden mode for the hadro-phobic scalar bosons. Since direct searches at high energy colliders provide independent information, the LHC exploration should continue.

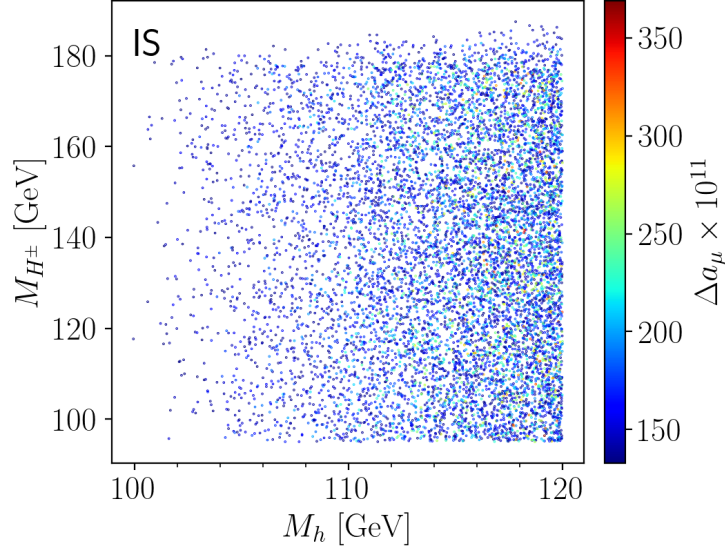


FIG. 8: The finally allowed (M_h, M_{H^\pm}) in the inverted scenario with the color code indicating the value of Δa_μ .

A. Electron anomalous magnetic moment

As a flavor universal theory, Type-X 2HDM has the same contributions to Δa_e and Δa_μ except the differences of the electron and muon masses. Positive Δa_μ demands positive Δa_e . In the measurement, however, Δa_e has not been settled yet because of the discrepancy in the recent two experiments for the fine structure constant α , the most sensitive input to Δa_e . Depending on whether we take the data from ^{133}Cs [86] or from ^{87}Rb [87], the deviations of the electron $g - 2$ from the SM prediction [46, 151, 152] are substantially different as

$$\begin{aligned}\Delta a_e^{\text{Cs}} &= -8.8(3.6) \times 10^{-13}, \\ \Delta a_e^{\text{Rb}} &= 4.8(3.0) \times 10^{-13}.\end{aligned}\tag{18}$$

At 2σ level, Δa_e^{Cs} is negative while Δa_e^{Rb} can be positive.

In Fig. 9, we present the Δa_e over the finally allowed (M_A, t_β) . The left (right) panel corresponds to the normal (inverted) scenario. The viable parameters predict $\Delta a_e \in [0.36, 1.17] \times 10^{-13}$ in the normal scenario and $\Delta a_e \in [0.33, 1.15] \times 10^{-13}$ in the inverted scenario. The Δa_e^{Rb} is explained at 2σ , except for the points along the upper-left boundary of the allowed (M_A, t_β) space. The Δa_e^{Cs} is negative at 2σ , which is contradictory to the prediction of the model. At 3σ , however, it is consistent with the model.

B. Production of the hadro-phobic new scalars at the LHC

For the LHC phenomenology, we point out two characteristics of the finally allowed parameters: (i) t_β is extremely large; (ii) the masses of new scalar bosons are below about 300 GeV.

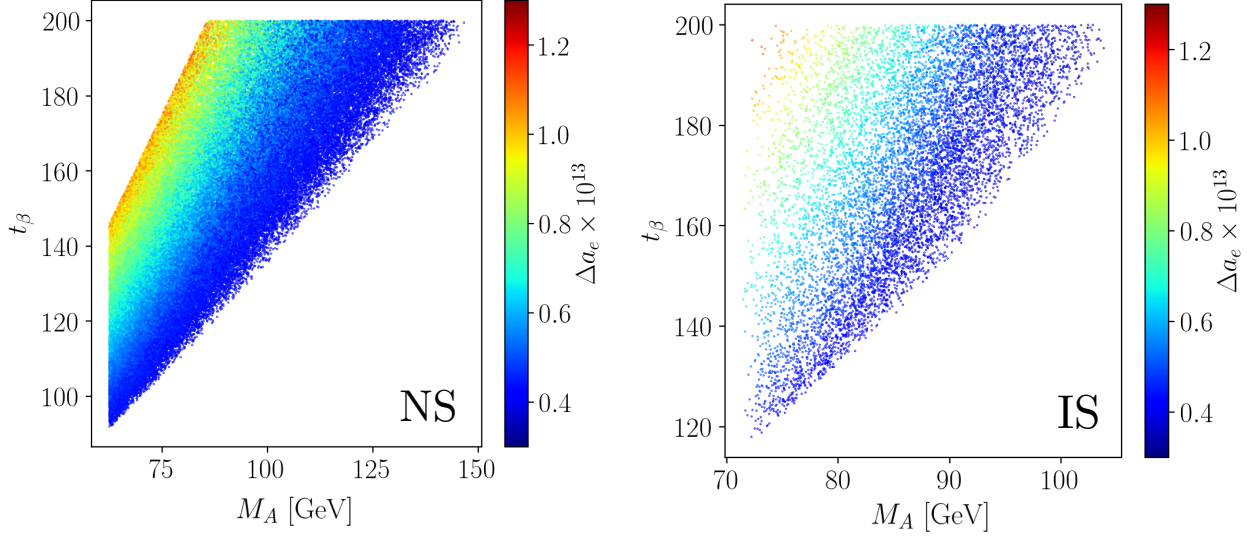


FIG. 9: Δa_e of the finally allowed parameter points that satisfy all the theoretical and experimental constraints including Δa_μ , projected on (M_A, t_β) . The left (right) panel corresponds to the normal (inverted) scenario.

The new scalar bosons with intermediate mass have escaped the LHC searches because of their hadro-phobic nature due to large t_β . For the intermediate-mass H^\pm , the current LHC search depends on its production via the decay of a top quark into bH^\pm , followed by $H^\pm \rightarrow \tau\nu$ [147, 148]. When $t_\beta \gtrsim 100$, however, the H^\pm - t - b vertex is extremely small, suppressing the production of the charged Higgs boson. For the intermediate-mass A and φ^0 , the LHC searches resort to the gluon fusion production via top quark loops, which is also suppressed. These hadro-phobic new scalar bosons need different search strategies.

We study the branching ratios of A , φ^0 , and H^\pm in the viable parameter space. Both A and φ^0 dominantly decay into $\tau^+\tau^-$. The branching ratios of $H \rightarrow ZA$ and $H \rightarrow H^\pm W^\mp$ are below 10%. For the H^\pm decays, Fig. 10 presents the scatter plot of the branching ratios as a function of $(M_{H^\pm} - M_A)$ in the normal (left panel) and inverted (right panel) scenario. The color code indicates the value of t_β . The primary decay channel of H^\pm is into $\tau^\pm\nu$. The second important mode is $H^\pm \rightarrow W^\pm A$, which is sizable for larger $(M_{H^\pm} - M_A)$ and smaller t_β . In the normal scenario, $\mathcal{B}(H^\pm \rightarrow W^\pm A)$ can reach up to about 30%. In the inverted scenario, its maximum is only about 3%.

Based on these characteristics, we consider the following two channels:

$$q\bar{q} \rightarrow Z^* \rightarrow A\varphi^0 \rightarrow \tau^+\tau^-\tau^+\tau^-, \quad (19)$$

$$pp \rightarrow H^+H^- \rightarrow \tau^+\nu\tau^-\nu. \quad (20)$$

The process in Eq. (19) is efficient since the Z - A - φ^0 vertex has the maximal value in the alignment limit of both scenarios. In addition, m_{φ^0} can be measured through the $\tau^+\tau^-$ invariant mass distribution, differentiating the normal scenario from the inverted scenario. The pair

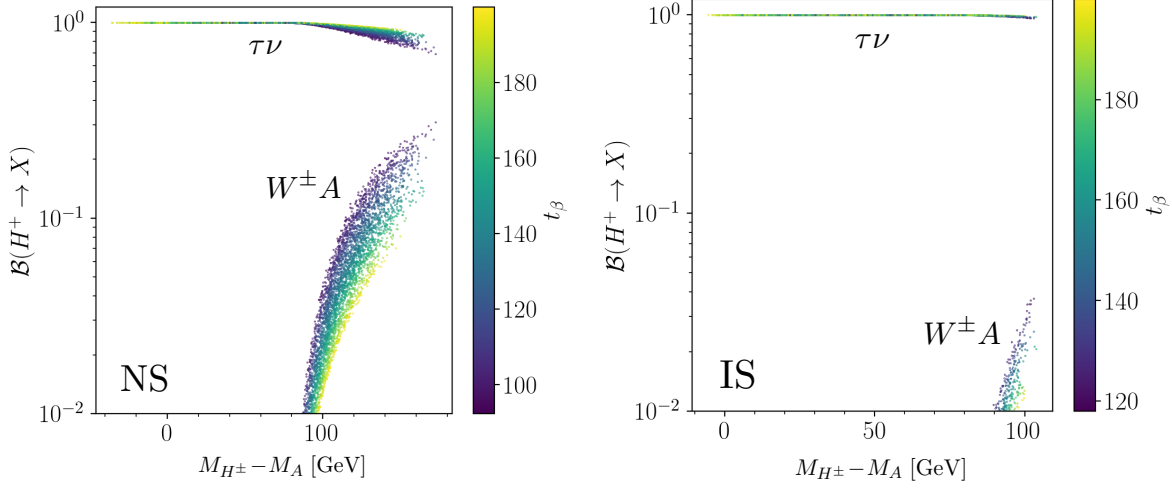


FIG. 10: The branching ratios of the charged Higgs boson as a function of $(M_{H^\pm} - M_A)$ for the finally allowed parameter points. The left (right) panel corresponds to the normal (inverted) scenario.

production of charged Higgs bosons in Eq. (20) is almost uniquely determined by M_{H^\pm} since the production is via the gauge couplings to γ and Z .

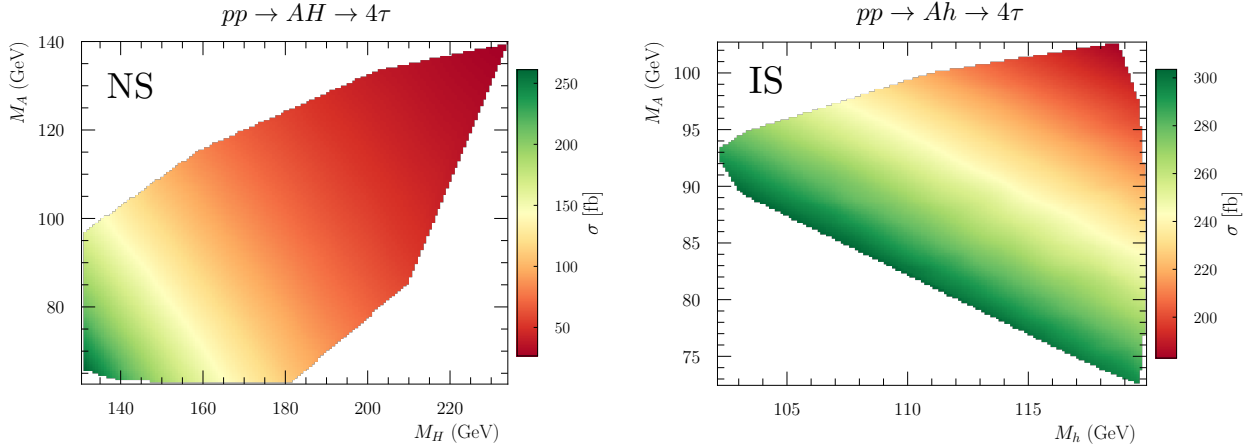


FIG. 11: The total cross section at the 14 TeV LHC for the process $pp \rightarrow Z^* \rightarrow AH/Ah \rightarrow 4\tau$ of the finally allowed parameter points, projected on $(M_H/M_h, t_\beta)$. The left (right) panel corresponds to the normal (inverted) scenario.

Figure 11 shows the parton-level total cross sections of $pp \rightarrow Z^* \rightarrow AH/Ah \rightarrow 4\tau$ at the 14 TeV LHC, by scanning all the viable parameter points. In both scenarios, we see a strong anti-correlation of σ_{tot} with $M_A + M_H$. In the normal scenario (left panel), the total cross section lies between ~ 25 fb and ~ 260 fb. In the inverted scenario, σ_{tot} goes up to about 300 fb, larger than in the normal scenario. Considering the observed $\sigma(pp \rightarrow ZZ \rightarrow 4\tau) \simeq 17$ fb at the 13 TeV LHC [153, 154], the process $pp \rightarrow A\varphi^0 \rightarrow 4\tau$ has a high potential to probe the model.

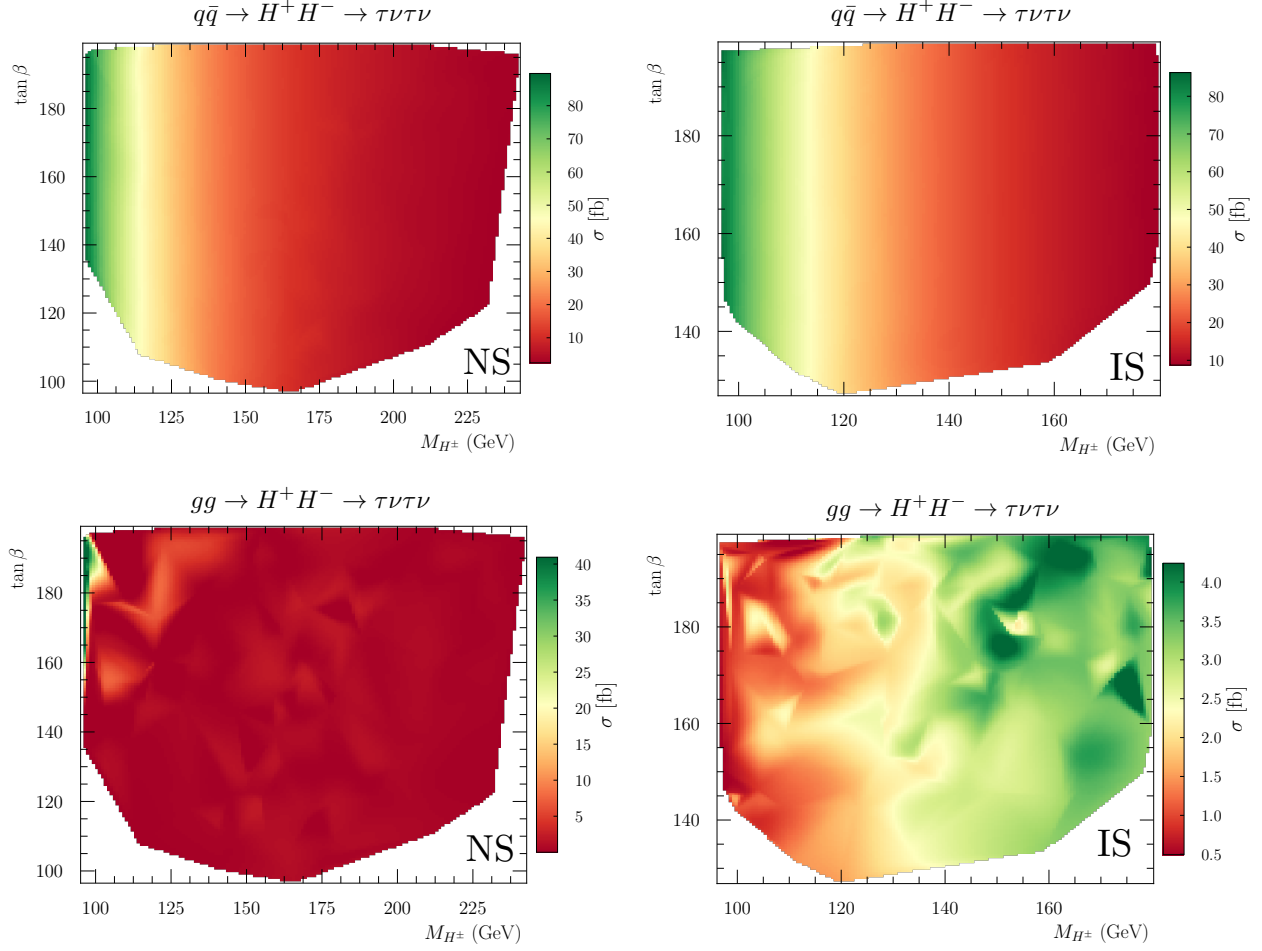


FIG. 12: The total cross section at the 14 TeV LHC for the process $pp \rightarrow H^+ H^- \rightarrow \tau \nu \tau \nu$ of the finally allowed parameter points, projected on (M_{H^\pm}, t_β) . The results in the normal (inverted) scenario are in the left (right) panels. Two upper panels correspond to $q\bar{q} \rightarrow H^+ H^-$, and two lower panels to the gluon fusion production.

In Fig. 12, we present the prediction of the viable parameters to the total cross sections of the process $pp \rightarrow H^+ H^- \rightarrow \tau \nu \tau \nu$ at the 14 TeV LHC. The results in the normal (inverted) scenario are in the left (right) panels. Two upper (lower) panels present the total cross sections for $q\bar{q} \rightarrow H^+ H^-$ ($gg \rightarrow H^+ H^-$). In most parameter spaces, the Drell-Yan production has a much larger signal rate, since the hadro-phobic nature of the charged Higgs boson suppresses the gluon fusion production mediated by the top quark loop. The irreducible backgrounds for the final state of $\tau^+ \nu \tau^- \nu$ are $pp \rightarrow W^+ W^- \rightarrow \tau^+ \nu \tau^- \nu$ and $pp \rightarrow ZZ \rightarrow \tau^+ \tau^- \nu \nu$. Considering $\sigma_{\text{tot}}^{\text{SM}}(pp \rightarrow W^+ W^- \rightarrow \tau^+ \nu \tau^- \nu) \simeq 1.7 \text{ pb}$ [155] and $\sigma_{\text{tot}}^{\text{SM}}(pp \rightarrow ZZ \rightarrow \tau^+ \tau^- \nu \nu) \simeq 100 \text{ fb}$ [153, 154] at the 13 TeV LHC, there is a chance to see the process.

VI. LEPTON FLAVOR UNIVERSALITY DATA IN THE τ AND Z DECAYS

In Sec. IV, we found that the Type-X 2HDM as a solution to the muon $g-2$ does not allow decoupling of any new Higgs boson. The generically flavor-universal model may yield excessive violation of the LFU in the τ and Z decays, through the loop contributions mediated by new Higgs bosons. For the rigorous analysis, we first categorize the LFU data as follows:

(i) HFLAV global fit results in the τ decay: To parameterize the LFU in the τ decays, we introduce the coupling ratios defined by

$$\begin{aligned} \left(\frac{g_\tau}{g_\mu}\right)^2 &\equiv \frac{\Gamma(\tau \rightarrow e\nu\nu)}{\Gamma(\mu \rightarrow e\nu\nu)} \times \frac{f(\rho_\mu^e)}{f(\rho_\tau^e)}, \\ \left(\frac{g_\tau}{g_e}\right)^2 &\equiv \frac{\Gamma(\tau \rightarrow \mu\nu\nu)}{\Gamma(\mu \rightarrow e\nu\nu)} \times \frac{f(\rho_\mu^e)}{f(\rho_\tau^\mu)}, \\ \left(\frac{g_\mu}{g_e}\right)^2 &\equiv \frac{\Gamma(\tau \rightarrow \mu\nu\nu)}{\Gamma(\tau \rightarrow e\nu\nu)} \times \frac{f(\rho_\tau^e)}{f(\rho_\tau^\mu)}, \end{aligned} \quad (21)$$

where $\rho_j^i = m_i^2/m_j^2$ and

$$f(x) = 1 - 8x + 8x^3 - x^4 - 12x^2 \ln x. \quad (22)$$

The second factors in the right-hand sides of Eq. (21) cancel the mass differences of the charged leptons. Including the hadronic decays of $\tau \rightarrow \pi\nu/K\nu \rightarrow \mu\nu\nu$, we consider

$$\mathcal{R}_1^\tau \equiv \frac{g_\tau}{g_\mu}, \quad \mathcal{R}_2^\tau \equiv \frac{g_\tau}{g_e}, \quad \mathcal{R}_3^\tau \equiv \frac{g_\mu}{g_e}, \quad \mathcal{R}_4^\tau \equiv \left(\frac{g_\tau}{g_\mu}\right)_\pi, \quad \mathcal{R}_5^\tau \equiv \left(\frac{g_\tau}{g_\mu}\right)_K, \quad (23)$$

where $(\mathcal{R}_{1,\dots,5}^\tau)^{\text{SM}} = 1$. Since $\mathcal{R}_2^\tau/\mathcal{R}_1^\tau = \mathcal{R}_3^\tau$, only four in Eq. (23) are independent. We should remove one redundant degree of freedom that has a zero eigenvalue in the covariance matrix.

(ii) Michel parameters: In the decay of $\tau^- \rightarrow \ell^- \nu \nu_\tau$, the energy and angular distribution of ℓ^- provides valuable information on the LFU. The distribution is written in terms of the Michel parameters ρ , η , ξ , and δ , as [156, 157]

$$\begin{aligned} \frac{d^2\Gamma}{dx d\cos\theta^*} \propto & x^2 \left[3(1-x) + \frac{2\rho}{3}(4x-3) + 3\eta x_0 \frac{1-x}{x} \right. \\ & \left. + P_\tau \xi \cos\theta^* \left\{ 1-x + \frac{2\delta}{3}(4x-3) \right\} \right], \end{aligned} \quad (24)$$

where $x = 2E_\ell/m_\tau$, $x_0 = 2m_\ell/m_\tau$, P_τ is the τ^- polarization, and θ^* is the angle between the ℓ^- momentum and the τ^- spin quantization axis. In the SM [158], they are³

$$\rho^{\text{SM}} = \frac{3}{4}, \quad \eta^{\text{SM}} = 0, \quad \xi^{\text{SM}} = 1, \quad (\xi\delta)^{\text{SM}} = \frac{3}{4}. \quad (25)$$

³ For the hadronic τ decay, only the ξ_h was measured. In the literature, two conventions for the sign of ξ_h coexist, $\xi_h > 0$ in Refs. [89, 158, 159] and $\xi_h < 0$ in Refs. [80, 160]. To unify with $\xi_\ell = 1$ from the leptonic τ decays, we adopt the positive ξ_h convention.

Including the leptonic and hadronic decays of τ^- , we consider the Michel parameters of

$$\begin{aligned}\mathcal{R}_1^{\text{M}} &\equiv \rho_e, & \mathcal{R}_2^{\text{M}} &\equiv (\xi\delta)_e, & \mathcal{R}_3^{\text{M}} &\equiv \xi_e, \\ \mathcal{R}_4^{\text{M}} &\equiv \eta_\mu, & \mathcal{R}_5^{\text{M}} &\equiv \rho_\mu, & \mathcal{R}_6^{\text{M}} &\equiv (\xi\delta)_\mu, & \mathcal{R}_7^{\text{M}} &\equiv \xi_\mu, \\ \mathcal{R}_8^{\text{M}} &\equiv \xi_\pi, & \mathcal{R}_9^{\text{M}} &\equiv \xi_\rho, & \mathcal{R}_{10}^{\text{M}} &\equiv \xi_{a_1}.\end{aligned}\quad (26)$$

(iii) **LFU in the Z decay:** From the partial decay rates of the leptonic Z decays, we take two ratios of [161]

$$\mathcal{R}_1^Z \equiv \frac{\Gamma(Z \rightarrow \mu^+ \mu^-)}{\Gamma(Z \rightarrow e^+ e^-)}, \quad \mathcal{R}_2^Z \equiv \frac{\Gamma(Z \rightarrow \tau^+ \tau^-)}{\Gamma(Z \rightarrow e^+ e^-)}.\quad (27)$$

where $(\mathcal{R}_{1,2}^Z)^{\text{SM}} = 1$ if neglecting m_τ^2/m_Z^2 .

The Type-X 2HDM makes two sorts of contributions to the observables in the τ decays, the tree-level contributions (mediated by the charged Higgs boson) and the one-loop level contributions. We parameterize them by

$$\begin{aligned}\delta_{\text{tree}} &= \frac{m_\mu m_\tau t_\beta^2}{M_{H^\pm}^2}, \\ \delta_{\text{loop}} &= \frac{1}{16\pi^2} \frac{m_\tau^2 t_\beta^2}{v^2} \left[1 + \frac{1}{4} \left\{ H(\rho_{H^\pm}^A) + H(\rho_{H^\pm}^{\varphi^0}) \right\} \right],\end{aligned}\quad (28)$$

where $\rho_j^i = m_i^2/m_j^2$, and $H(x) = (1+x) \ln x / (1-x)$. If $M_A = M_H = M_{H^\pm}$, we have $\delta_{\text{loop}} = 0$ since $\lim_{x \rightarrow 1} H(x) = -2$. Therefore, similar masses of H , A , and H^\pm in the viable parameter space help to suppress the loop-corrections to the τ decays.

For the HFLAV results, \mathcal{R}_i^τ 's in Eq. (23) receive new contributions, given by

$$\begin{aligned}\mathcal{R}_1^\tau &= \mathcal{R}_4^\tau = \mathcal{R}_5^\tau = 1 + \epsilon_{\text{loop}}^\tau, \\ \mathcal{R}_2^\tau &= 1 + \delta_{\text{loop}} + \epsilon_{\text{tree}}^\tau, \\ \mathcal{R}_3^\tau &= 1 + \epsilon_{\text{tree}}^\tau.\end{aligned}\quad (29)$$

Here $\epsilon_{\text{tree}}^\tau$ is

$$\epsilon_{\text{tree}}^\tau = \delta_{\text{tree}} \left[\frac{\delta_{\text{tree}}}{8} - \frac{m_\mu}{m_\tau} \frac{g(\rho_\tau^\mu)}{f(\rho_\tau^\mu)} \right],\quad (30)$$

where $g(x) = 1 + 9x - 9x^2 - x^3 + 6x(1+x) \ln x$ and $f(x)$ is in Eq. (22).

For the Michel parameters, only the η_μ , $(\xi\delta)_\mu$, and ξ_μ are modified as

$$\begin{aligned}\mathcal{R}_4^{\text{M}} &\equiv \eta_\mu = -\frac{2\delta_{\text{tree}}(1 + \delta_{\text{loop}})}{4 + \delta_{\text{tree}}^2}, \\ \mathcal{R}_6^{\text{M}} &\equiv (\xi\delta)_\mu = \frac{3}{4} \times \frac{4(1 + \delta_{\text{loop}})^2 - \delta_{\text{tree}}^2}{4(1 + \delta_{\text{loop}})^2 + \delta_{\text{tree}}^2}, \\ \mathcal{R}_7^{\text{M}} &\equiv \xi_\mu = \frac{4(1 + \delta_{\text{loop}})^2 - \delta_{\text{tree}}^2}{4(1 + \delta_{\text{loop}})^2 + \delta_{\text{tree}}^2}.\end{aligned}\quad (31)$$

The corrections to ρ_e , $(\xi\delta)_e$, and ξ_e are suppressed by the small electron mass. For the hadronic τ decays, the corrections are independent of t_β , which is much smaller in the large t_β limit than the t_β^2 corrections in the leptonic τ decays.

For \mathcal{R}_i^Z 's, new contributions are written as

$$\mathcal{R}_i^Z - 1 = \frac{2g_L^{\text{SM}}\text{Re}(\delta g_L^i) + 2g_R^{\text{SM}}\text{Re}(\delta g_R^i)}{(g_L^{\text{SM}})^2 + (g_R^{\text{SM}})^2}, \quad (i = \mu, \tau) \quad (32)$$

where $g_L^{\text{SM}} = s_W^2 - 1/2$, $g_R^{\text{SM}} = s_W^2$, and the full expressions for $\delta g_{L/R}^{\mu, \tau}$ at one-loop level are referred to Ref. [80].

Rough estimation of new contributions is useful. Since $\delta_{\text{tree}} \gg \delta_{\text{loop}}$ and $\delta_{\text{tree}} \gg \epsilon_{\text{tree}}^\tau$, the dominant contribution is

$$\eta_\mu \simeq -\frac{1}{2}\delta_{\text{tree}}. \quad (33)$$

While δ_{tree} is positive so that $\eta_\mu < 0$ in the model, the ALEPH result is $\eta_\mu^{\text{ALEPH}} = 0.160 \pm 0.150$ [89]. The observed η_μ threatens the consistency of the Type-X 2HDM with the LFU data.

Now we perform the global χ^2 fit of the Type-X 2HDM to

$$\Delta a_\mu, \quad \mathcal{R}_{1, \dots, 5}^\tau, \quad \mathcal{R}_{1, \dots, 10}^{\text{M}}, \quad \mathcal{R}_{1, 2}^Z. \quad (34)$$

The experimental results of \mathcal{R} 's and the correlation matrices are summarized in Appendix A. Altogether we have 17 independent observables, $N_{\text{obs}} = 17$, since we removed one redundant degree of freedom in $\mathcal{R}_{1, \dots, 5}^\tau$. In the SM where the number of degree of freedom is $N_{\text{dof}} = 17$, χ_{min}^2 and p value are

$$\chi_{\text{min}}^2(\text{SM}) = 37.3, \quad p(\text{SM}) = 0.003. \quad (35)$$

The $\Delta a_\mu^{\text{obs}}$ with the LFU data calls for NP.

For the Type-X 2HDM, we address two issues. The first is the number of degrees of freedom, $N_{\text{dof}} = N_{\text{obs}} - N_{\text{par}}$, where N_{par} is the number of free parameters. We subtract N_{par} under the assumption that we use one free parameter to explain one observable. But our hypothesis model is not a *free* Type-X 2HDM. It is the model severely limited by the theoretical and experimental constraints. In favor of the Type-X 2HDM, we take $N_{\text{dof}} = 17$. The second issue is the range of the model parameters in the global χ^2 fit. When finding χ_{min}^2 , we may scan either the whole parameter space without imposing other constraints or only the parameter space consistent with all the constraints. In the two cases, p -values show big differences as follows:

$$\begin{aligned} p(\text{NS: Step I}) &= 0.58, & p(\text{NS: Step III}) &= 0.02, \\ p(\text{IS: Step I}) &= 0.059, & p(\text{IS: Step III}) &= 0.02. \end{aligned} \quad (36)$$

Without the LHC data, the Type-X 2HDM in both scenarios well explains the Δa_μ and LFU data. With the combination of the LHC data and LFU data, however, the model is excluded as a solution to the new Fermilab measurement of the muon $g - 2$.

VII. CONCLUSION

In light of the recent measurement of the muon anomalous magnetic moment by Fermilab Muon $g - 2$ experiment, we comprehensively study the Type-X (Lepton-specific) two Higgs doublet model (2HDM). Beyond explaining only the observed Δa_μ , we included the theoretical stability conditions and almost all the available experimental results in the analysis. Since the Higgs precision data prefers the SM-like Higgs boson, more strongly for large t_β , we assumed the Higgs alignment. Two possible scenarios are studied, the normal scenario where the lighter CP -even h becomes h_{SM} and the inverted scenario where the heavier CP -even H is h_{SM} . The model has five parameters, m_{φ^0} , M_A , M_{H^\pm} , M^2 , and t_β , where $\varphi^0 = H$ in the normal scenario and $\varphi^0 = h$ in the inverted scenario.

Various phenomenological conditions cause a chain reaction of constraining the model parameters. First, the large and positive $\Delta a_\mu^{\text{obs}}$ requires large t_β and light M_A . The dominant contribution is from the τ^\pm loop mediated by A in the two-loop Barr-Zee diagram. Unwanted is the negative contribution of φ^0 to the τ^\pm loop in the Barr-Zee diagram. But decoupling of φ^0 conflicts with the theoretical stability because of large t_β . The Higgs quartic coupling λ_1 has t_β^2 terms, which can easily break the perturbativity of λ_1 . Requiring the t_β^2 terms to vanish yields $m_{\varphi^0}^2 \approx M^2$. Perturbativity of other quartic couplings subsequently demands $M_A \simeq M_{H^\pm} \simeq M \approx m_{\varphi^0}$. Decoupling of any new Higgs boson is not possible. The direct search bounds at the LEP and LHC exclude a large portion of the parameter space: $pp \rightarrow h_{\text{SM}} \rightarrow AA$ in the normal scenario and $e^+e^- \rightarrow Z^* \rightarrow Ah$ in the inverted scenario are the smoking signals. Only the region with $M_A > m_{h_{\text{SM}}}/2$ survives. In turn, $\Delta a_\mu^{\text{obs}}$ demands $t_\beta \gtrsim 100$.

Through random scanning without any prior assumptions on the masses and couplings, we obtained the parameter points consistent with the muon $g - 2$, theoretical stabilities, $S/T/U$ parameters, Higgs precision data, and direct search results. We also studied the phenomenological implications of the allowed parameter space. The model prediction to the electron anomalous magnetic moment is consistent with the observation, Δa_e^{Cs} (using the fine structure constant α from ^{133}Cs) at 3σ , and Δa_e^{Rb} (using α from ^{87}Rb) at 2σ . For the HL-LHC searches, we calculated the total cross sections for the hadro-phobic new scalar bosons in two processes, $pp \rightarrow A\varphi^0 \rightarrow 4\tau$ and $pp \rightarrow H^+H^- \rightarrow \tau\nu\tau\nu$. In particular, $pp \rightarrow A\varphi^0 \rightarrow 4\tau$ has the total cross section around $25 \sim 260$ fb in the normal scenario and $180 \sim 300$ fb in the inverted scenario. The model has a high potential to be probed at the LHC. As the final check of the model, we studied the lepton flavor universality in the τ and Z decays. Through a global χ^2 fit to 16 LFU data and $\Delta a_\mu^{\text{obs}}$, we showed that the combination of the LHC results and the LFU data excludes the Type-X 2HDM as a solution to the muon $g - 2$.

The confirmed deviation of the muon $g - 2$ from the SM prediction by the recent Fermilab experiment indicates the dawn of a new physics era. The Type-X 2HDM that explains Δa_μ is consistent with the LEP and LHC data in limited parameter space, but not with the LFU data in the τ and Z decays. The future LHC searches targeting the specific parameters shall provide a valuable and independent probe of the model, which we strongly support.

Acknowledgments

We would like to thank Kingman Cheung and Chih-Ting Lu for useful discussions. This work is supported by the National Research Foundation of Korea, Grant No. NRF-2019R1A2C1009419.

Appendix A: Used parameters in the τ^\pm and Z decays for the global χ^2 analysis

We present the experimental data on the parameters in the τ^\pm and Z decays, which were used in the global χ^2 analysis of Sec. VI.

(i) HFLAV global fit results in the τ decay: [88]

$$\begin{aligned}
\mathcal{R}_1^\tau &\equiv \left(\frac{g_\tau}{g_\mu} \right) = 1.0010 \pm 0.0014, \\
\mathcal{R}_2^\tau &\equiv \left(\frac{g_\tau}{g_e} \right) = 1.0029 \pm 0.0014, \\
\mathcal{R}_3^\tau &\equiv \left(\frac{g_\mu}{g_e} \right) = 1.0018 \pm 0.0014, \\
\mathcal{R}_4^\tau &\equiv \left(\frac{g_\tau}{g_\mu} \right)_\pi = 0.9958 \pm 0.0026, \\
\mathcal{R}_5^\tau &\equiv \left(\frac{g_\tau}{g_\mu} \right)_K = 0.9879 \pm 0.0063,
\end{aligned} \tag{A1}$$

and the correlation matrix for $(\mathcal{R}_1^\tau, \dots, \mathcal{R}_5^\tau)$ is

$$(\boldsymbol{\rho}_{ij}^\tau) = \begin{pmatrix} 1.00 & 0.51 & -0.50 & 0.23 & 0.11 \\ 0.51 & 1.00 & 0.49 & 0.25 & 0.10 \\ -0.50 & 0.49 & 1.00 & 0.02 & -0.01 \\ 0.23 & 0.25 & 0.02 & 1.00 & 0.06 \\ 0.11 & 0.10 & -0.01 & 0.06 & 1.00 \end{pmatrix}. \tag{A2}$$

(ii) Michel parameters in the τ decay: [89]

$$\begin{aligned}
\mathcal{R}_1^{\text{M}} &\equiv \rho_e = 0.747 \pm 0.019, \\
\mathcal{R}_2^{\text{M}} &\equiv (\xi\delta)_e = 0.788 \pm 0.066, \\
\mathcal{R}_3^{\text{M}} &\equiv \xi_e = 1.011 \pm 0.094, \\
\mathcal{R}_4^{\text{M}} &\equiv \eta_\mu = 0.160 \pm 0.150, \\
\mathcal{R}_5^{\text{M}} &\equiv \rho_\mu = 0.776 \pm 0.045, \\
\mathcal{R}_6^{\text{M}} &\equiv (\xi\delta)_\mu = 0.786 \pm 0.066, \\
\mathcal{R}_7^{\text{M}} &\equiv \xi_\mu = 1.030 \pm 0.120, \\
\mathcal{R}_8^{\text{M}} &\equiv \xi_\pi = 0.994 \pm 0.020, \\
\mathcal{R}_9^{\text{M}} &\equiv \xi_\rho = 0.987 \pm 0.012, \\
\mathcal{R}_{10}^{\text{M}} &\equiv \xi_{a_1} = 1.000 \pm 0.016.
\end{aligned} \tag{A3}$$

and the correlation matrix for $(\mathcal{R}_1^{\text{M}}, \dots, \mathcal{R}_{10}^{\text{M}})$ is

$$(\rho_{ij}^{\text{M}}) = \begin{pmatrix} 1.00 & 0.00 & -0.23 & -0.02 & 0.02 & 0.00 & -0.02 & 0.10 & 0.00 & 0.00 \\ 0.00 & 1.00 & 0.05 & 0.01 & 0.00 & 0.00 & -0.02 & -0.12 & 0.01 & 0.01 \\ -0.23 & 0.05 & 1.00 & 0.01 & 0.01 & -0.02 & -0.01 & -0.06 & -0.02 & -0.01 \\ -0.02 & 0.01 & 0.01 & 1.00 & 0.91 & 0.29 & 0.58 & 0.03 & -0.02 & -0.01 \\ 0.02 & 0.00 & 0.01 & 0.91 & 1.00 & 0.25 & 0.45 & 0.06 & -0.02 & -0.01 \\ 0.00 & 0.00 & -0.02 & 0.29 & 0.25 & 1.00 & 0.14 & -0.07 & -0.02 & -0.01 \\ -0.02 & -0.02 & -0.01 & 0.58 & 0.45 & 0.14 & 1.00 & -0.01 & -0.04 & -0.02 \\ 0.10 & -0.12 & -0.06 & 0.03 & 0.06 & -0.07 & -0.01 & 1.00 & -0.28 & -0.20 \\ 0.00 & 0.01 & -0.02 & -0.02 & -0.02 & -0.02 & -0.04 & -0.28 & 1.00 & -0.08 \\ 0.00 & 0.01 & -0.01 & -0.01 & -0.01 & -0.01 & -0.02 & -0.20 & -0.08 & 1.00 \end{pmatrix}. \tag{A4}$$

(iii) LFU in the Z decay: [161]

$$\begin{aligned}
\mathcal{R}_1^Z &\equiv \frac{\Gamma(Z \rightarrow \mu^+ \mu^-)}{\Gamma(Z \rightarrow e^+ e^-)} = 1.0009 \pm 0.0028, \\
\mathcal{R}_2^Z &\equiv \frac{\Gamma(Z \rightarrow \tau^+ \tau^-)}{\Gamma(Z \rightarrow e^+ e^-)} = 1.0019 \pm 0.0032,
\end{aligned} \tag{A5}$$

where the correlation between \mathcal{R}_1^Z and \mathcal{R}_2^Z is +0.63.

-
- [1] MUON G-2 collaboration, B. Abi et al., *Measurement of the Positive Muon Anomalous Magnetic Moment to 0.46 ppm*, *Phys. Rev. Lett.* **126** (2021) 141801, [2104.03281].
- [2] T. Albahri et al., *Measurement of the anomalous precession frequency of the muon in the Fermilab Muon g-2 experiment*, *Phys. Rev. D* **103** (2021) 072002, [2104.03247].

- [3] MUON G-2 collaboration, G. W. Bennett et al., *Final Report of the Muon E821 Anomalous Magnetic Moment Measurement at BNL*, *Phys. Rev. D* **73** (2006) 072003, [[hep-ex/0602035](#)].
- [4] T. Aoyama, M. Hayakawa, T. Kinoshita and M. Nio, *Complete Tenth-Order QED Contribution to the Muon $g-2$* , *Phys. Rev. Lett.* **109** (2012) 111808, [[1205.5370](#)].
- [5] A. Czarnecki, W. J. Marciano and A. Vainshtein, *Refinements in electroweak contributions to the muon anomalous magnetic moment*, *Phys. Rev. D* **67** (2003) 073006, [[hep-ph/0212229](#)].
- [6] C. Gnendiger, D. Stöckinger and H. Stöckinger-Kim, *The electroweak contributions to $(g-2)_\mu$ after the Higgs boson mass measurement*, *Phys. Rev. D* **88** (2013) 053005, [[1306.5546](#)].
- [7] A. Kurz, T. Liu, P. Marquard and M. Steinhauser, *Hadronic contribution to the muon anomalous magnetic moment to next-to-next-to-leading order*, *Phys. Lett. B* **734** (2014) 144–147, [[1403.6400](#)].
- [8] M. Davier, A. Hoecker, B. Malaescu and Z. Zhang, *Reevaluation of the hadronic vacuum polarisation contributions to the Standard Model predictions of the muon $g-2$ and $\alpha(m_Z^2)$ using newest hadronic cross-section data*, *Eur. Phys. J. C* **77** (2017) 827, [[1706.09436](#)].
- [9] G. Colangelo, M. Hoferichter and P. Stoffer, *Two-pion contribution to hadronic vacuum polarization*, *JHEP* **02** (2019) 006, [[1810.00007](#)].
- [10] A. Keshavarzi, D. Nomura and T. Teubner, *Muon $g-2$ and $\alpha(M_Z^2)$: a new data-based analysis*, *Phys. Rev. D* **97** (2018) 114025, [[1802.02995](#)].
- [11] A. Keshavarzi, D. Nomura and T. Teubner, *$g-2$ of charged leptons, $\alpha(M_Z^2)$, and the hyperfine splitting of muonium*, *Phys. Rev. D* **101** (2020) 014029, [[1911.00367](#)].
- [12] M. Davier, A. Hoecker, B. Malaescu and Z. Zhang, *A new evaluation of the hadronic vacuum polarisation contributions to the muon anomalous magnetic moment and to $\alpha(m_Z^2)$* , *Eur. Phys. J. C* **80** (2020) 241, [[1908.00921](#)].
- [13] B.-L. Hoid, M. Hoferichter and B. Kubis, *Hadronic vacuum polarization and vector-meson resonance parameters from $e^+e^- \rightarrow \pi^0\gamma$* , *Eur. Phys. J. C* **80** (2020) 988, [[2007.12696](#)].
- [14] G. Colangelo, M. Hoferichter and P. Stoffer, *Constraints on the two-pion contribution to hadronic vacuum polarization*, *Phys. Lett. B* **814** (2021) 136073, [[2010.07943](#)].
- [15] K. Melnikov and A. Vainshtein, *Hadronic light-by-light scattering contribution to the muon anomalous magnetic moment revisited*, *Phys. Rev. D* **70** (2004) 113006, [[hep-ph/0312226](#)].
- [16] G. Colangelo, M. Hoferichter, B. Kubis, M. Procura and P. Stoffer, *Towards a data-driven analysis of hadronic light-by-light scattering*, *Phys. Lett. B* **738** (2014) 6–12, [[1408.2517](#)].
- [17] G. Colangelo, M. Hoferichter, A. Nyffeler, M. Passera and P. Stoffer, *Remarks on higher-order hadronic corrections to the muon $g-2$* , *Phys. Lett. B* **735** (2014) 90–91, [[1403.7512](#)].
- [18] G. Colangelo, M. Hoferichter, M. Procura and P. Stoffer, *Dispersion relation for hadronic light-by-light scattering: theoretical foundations*, *JHEP* **09** (2015) 074, [[1506.01386](#)].
- [19] G. Colangelo, M. Hoferichter, M. Procura and P. Stoffer, *Dispersion relation for hadronic light-by-light scattering: two-pion contributions*, *JHEP* **04** (2017) 161, [[1702.07347](#)].
- [20] P. Masjuan and P. Sanchez-Puertas, *Pseudoscalar-pole contribution to the $(g_\mu-2)$: a rational approach*, *Phys. Rev. D* **95** (2017) 054026, [[1701.05829](#)].

- [21] G. Colangelo, M. Hoferichter, M. Procura and P. Stoffer, *Rescattering effects in the hadronic-light-by-light contribution to the anomalous magnetic moment of the muon*, *Phys. Rev. Lett.* **118** (2017) 232001, [[1701.06554](#)].
- [22] M. Hoferichter, B.-L. Hoid, B. Kubis, S. Leupold and S. P. Schneider, *Pion-pole contribution to hadronic light-by-light scattering in the anomalous magnetic moment of the muon*, *Phys. Rev. Lett.* **121** (2018) 112002, [[1805.01471](#)].
- [23] M. Hoferichter, B.-L. Hoid, B. Kubis, S. Leupold and S. P. Schneider, *Dispersion relation for hadronic light-by-light scattering: pion pole*, *JHEP* **10** (2018) 141, [[1808.04823](#)].
- [24] G. Colangelo, F. Hagelstein, M. Hoferichter, L. Laub and P. Stoffer, *Short-distance constraints on hadronic light-by-light scattering in the anomalous magnetic moment of the muon*, *Phys. Rev. D* **101** (2020) 051501, [[1910.11881](#)].
- [25] J. Bijnens, N. Hermansson-Truedsson and A. Rodríguez-Sánchez, *Short-distance constraints for the HLbL contribution to the muon anomalous magnetic moment*, *Phys. Lett. B* **798** (2019) 134994, [[1908.03331](#)].
- [26] T. Blum, N. Christ, M. Hayakawa, T. Izubuchi, L. Jin, C. Jung et al., *Hadronic Light-by-Light Scattering Contribution to the Muon Anomalous Magnetic Moment from Lattice QCD*, *Phys. Rev. Lett.* **124** (2020) 132002, [[1911.08123](#)].
- [27] J. Bijnens, N. Hermansson-Truedsson, L. Laub and A. Rodríguez-Sánchez, *Short-distance HLbL contributions to the muon anomalous magnetic moment beyond perturbation theory*, *JHEP* **10** (2020) 203, [[2008.13487](#)].
- [28] S. Borsanyi et al., *Leading hadronic contribution to the muon $g - 2$ magnetic moment from lattice QCD*, [2002.12347](#).
- [29] C. Lehner and A. S. Meyer, *Consistency of hadronic vacuum polarization between lattice QCD and the R -ratio*, *Phys. Rev. D* **101** (2020) 074515, [[2003.04177](#)].
- [30] A. Crivellin, M. Hoferichter, C. A. Manzari and M. Montull, *Hadronic Vacuum Polarization: $(g - 2)_\mu$ versus Global Electroweak Fits*, *Phys. Rev. Lett.* **125** (2020) 091801, [[2003.04886](#)].
- [31] A. Keshavarzi, W. J. Marciano, M. Passera and A. Sirlin, *Muon $g - 2$ and $\Delta\alpha$ connection*, *Phys. Rev. D* **102** (2020) 033002, [[2006.12666](#)].
- [32] B. Malaescu and M. Schott, *Impact of correlations between a_μ and α_{QED} on the EW fit*, *Eur. Phys. J. C* **81** (2021) 46, [[2008.08107](#)].
- [33] A. Czarnecki and W. J. Marciano, *The Muon anomalous magnetic moment: A Harbinger for 'new physics'*, *Phys. Rev. D* **64** (2001) 013014, [[hep-ph/0102122](#)].
- [34] H. Baer, V. Barger and H. Serce, *Anomalous muon magnetic moment, supersymmetry, naturalness, LHC search limits and the landscape*, [2104.07597](#).
- [35] A. Aboubrahim, M. Klasen and P. Nath, *What Fermilab $(g - 2)_\mu$ experiment tells us about discovering SUSY at HL-LHC and HE-LHC*, [2104.03839](#).
- [36] J. Cao, J. Lian, Y. Pan, D. Zhang and P. Zhu, *Improved $(g - 2)_\mu$ Measurement and Singlino dark matter in the general NMSSM*, [2104.03284](#).
- [37] F. Wang, L. Wu, Y. Xiao, J. M. Yang and Y. Zhang, *GUT-scale constrained SUSY in light of*

- E989 muon $g-2$ measurement*, [2104.03262](#).
- [38] M. Van Beekveld, W. Beenakker, M. Schutten and J. De Wit, *Dark matter, fine-tuning and $(g-2)_\mu$ in the pMSSM*, [2104.03245](#).
 - [39] M. Abdughani, Y.-Z. Fan, L. Feng, Y.-L. Sming Tsai, L. Wu and Q. Yuan, *A common origin of muon $g-2$ anomaly, Galaxy Center GeV excess and AMS-02 anti-proton excess in the NMSSM*, [2104.03274](#).
 - [40] S. Baum, M. Carena, N. R. Shah and C. E. M. Wagner, *The Tiny $(g-2)$ Muon Wobble from Small- μ Supersymmetry*, [2104.03302](#).
 - [41] W. Ahmed, I. Khan, J. Li, T. Li, S. Raza and W. Zhang, *The Natural Explanation of the Muon Anomalous Magnetic Moment via the Electroweak Supersymmetry from the GmSUGRA in the MSSM*, [2104.03491](#).
 - [42] H.-B. Zhang, C.-X. Liu, J.-L. Yang and T.-F. Feng, *Muon anomalous magnetic dipole moment in the $\mu\nu$ SSM*, [2104.03489](#).
 - [43] M. Chakraborti, L. Roszkowski and S. Trojanowski, *GUT-constrained supersymmetry and dark matter in light of the new $(g-2)_\mu$ determination*, [2104.04458](#).
 - [44] P. Athron, C. Balázs, D. H. Jacob, W. Kotlarski, D. Stöckinger and H. Stöckinger-Kim, *New physics explanations of a_μ in light of the FNAL muon $g-2$ measurement*, [2104.03691](#).
 - [45] W. Yin, *Muon $g-2$ Anomaly in Anomaly Mediation*, [2104.03259](#).
 - [46] A. J. Buras, A. Crivellin, F. Kirk, C. A. Manzari and M. Montull, *Global Analysis of Leptophilic Z' Bosons*, [2104.07680](#).
 - [47] E. J. Chun and T. Mondal, *Leptophilic bosons and muon $g-2$ at lepton colliders*, [2104.03701](#).
 - [48] J. Liu, C. E. M. Wagner and X.-P. Wang, *A light complex scalar for the electron and muon anomalous magnetic moments*, *JHEP* **03** (2019) 008, [[1810.11028](#)].
 - [49] A. E. Cárcamo Hernández, S. Kovalenko, M. Maniatis and I. Schmidt, *Fermion mass hierarchy and $g-2$ anomalies in an extended 3HDM Model*, [2104.07047](#).
 - [50] K. Ban, Y. Jho, Y. Kwon, S. C. Park, S. Park and P.-Y. Tseng, *A comprehensive study of vector leptoquark on the B -meson and Muon $g-2$ anomalies*, [2104.06656](#).
 - [51] M. Du, J. Liang, Z. Liu and V. Q. Tran, *A vector leptoquark interpretation of the muon $g-2$ and B anomalies*, [2104.05685](#).
 - [52] D. Borah, M. Dutta, S. Mahapatra and N. Sahu, *Muon $(g-2)$ and XENON1T Excess with Boosted Dark Matter in $L_\mu - L_\tau$ Model*, [2104.05656](#).
 - [53] L. Zu, X. Pan, L. Feng, Q. Yuan and Y.-Z. Fan, *Constraining $U(1)_{L_\mu - L_\tau}$ charged dark matter model for muon $g-2$ anomaly with AMS-02 electron and positron data*, [2104.03340](#).
 - [54] J.-L. Yang, H.-B. Zhang, C.-X. Liu, X.-X. Dong and T.-F. Feng, *Muon $(g-2)$ in the B -LSSM*, [2104.03542](#).
 - [55] A. Greljo, P. Stangl and A. E. Thomsen, *A Model of Muon Anomalies*, [2103.13991](#).
 - [56] B. Zhu and X. Liu, *Probing light dark matter with scalar mediator: muon $(g-2)$ deviation, the proton radius puzzle*, [2104.03238](#).
 - [57] P. Escribano, J. Terol-Calvo and A. Vicente, *$(g-2)_{e,\mu}$ in an extended inverse type-III seesaw*,

2104.03705.

- [58] G. Arcadi, L. Calibbi, M. Fedele and F. Mescia, *Muon $g-2$ and B -anomalies from Dark Matter*, 2104.03228.
- [59] A. Crivellin and M. Hoferichter, *Consequences of chirally enhanced explanations of $(g-2)_\mu$ for $h \rightarrow \mu\mu$ and $Z \rightarrow \mu\mu$* , 2104.03202.
- [60] M. A. Buen-Abad, J. Fan, M. Reece and C. Sun, *Challenges for an axion explanation of the muon $g-2$ measurement*, 2104.03267.
- [61] S.-F. Ge, X.-D. Ma and P. Pasquini, *Probing the Dark Axion Portal with Muon Anomalous Magnetic Moment*, 2104.03276.
- [62] P. M. Ferreira, B. L. Gonçalves, F. R. Joaquim and M. Sher, *$(g-2)_\mu$ in the 2HDM and slightly beyond – an updated view*, 2104.03367.
- [63] X.-F. Han, T. Li, H.-X. Wang, L. Wang and Y. Zhang, *Lepton-specific inert two-Higgs-doublet model confronted with the new results for muon and electron $g-2$ anomalies and multi-lepton searches at the LHC*, 2104.03227.
- [64] C.-H. Chen, C.-W. Chiang and T. Nomura, *Muon $g-2$ in two-Higgs-doublet model with type-II seesaw mechanism*, 2104.03275.
- [65] N. Ghosh and J. Lahiri, *Revisiting a generalized two-Higgs-doublet model in light of the muon anomaly and lepton flavor violating decays at the HL-LHC*, *Phys. Rev. D* **103** (2021) 055009, [2010.03590].
- [66] N. Ghosh and J. Lahiri, *Generalized 2HDM with wrong-sign lepton Yukawa coupling, in light of $g_\mu-2$ and lepton flavor violation at the future LHC*, 2103.10632.
- [67] S.-P. Li, X.-Q. Li, Y.-Y. Li, Y.-D. Yang and X. Zhang, *Power-aligned 2HDM: a correlative perspective on $(g-2)_{e,\mu}$* , *JHEP* **01** (2021) 034, [2010.02799].
- [68] F. J. Botella, F. Cornet-Gomez and M. Nebot, *Electron and muon $g-2$ anomalies in general flavour conserving two Higgs doublets models*, *Phys. Rev. D* **102** (2020) 035023, [2006.01934].
- [69] S. Jana, V. P. K. and S. Saad, *Resolving electron and muon $g-2$ within the 2HDM*, *Phys. Rev. D* **101** (2020) 115037, [2003.03386].
- [70] S. Jana, P. K. Vishnu, W. Rodejohann and S. Saad, *Dark matter assisted lepton anomalous magnetic moments and neutrino masses*, *Phys. Rev. D* **102** (2020) 075003, [2008.02377].
- [71] D. Anselmi, K. Kannike, C. Marzo, L. Marzola, A. Melis, K. Mürsepp et al., *A fake doublet solution to the muon anomalous magnetic moment*, 2104.03249.
- [72] V. Keus, N. Koivunen and K. Tuominen, *Singlet scalar and 2HDM extensions of the Standard Model: CP-violation and constraints from $(g-2)_\mu$ and e EDM*, *JHEP* **09** (2018) 059, [1712.09613].
- [73] D. Sabatta, A. S. Cornell, A. Goyal, M. Kumar, B. Mellado and X. Ruan, *Connecting muon anomalous magnetic moment and multi-lepton anomalies at LHC*, *Chin. Phys. C* **44** (2020) 063103, [1909.03969].
- [74] K. Schmidt-Hoberg, F. Staub and M. W. Winkler, *Constraints on light mediators: confronting dark matter searches with B physics*, *Phys. Lett. B* **727** (2013) 506–510, [1310.6752].

- [75] J. Cao, P. Wan, L. Wu and J. M. Yang, *Lepton-Specific Two-Higgs Doublet Model: Experimental Constraints and Implication on Higgs Phenomenology*, *Phys. Rev. D* **80** (2009) 071701, [[0909.5148](#)].
- [76] A. Broggio, E. J. Chun, M. Passera, K. M. Patel and S. K. Vempati, *Limiting two-Higgs-doublet models*, *JHEP* **11** (2014) 058, [[1409.3199](#)].
- [77] L. Wang and X.-F. Han, *A light pseudoscalar of 2HDM confronted with muon $g-2$ and experimental constraints*, *JHEP* **05** (2015) 039, [[1412.4874](#)].
- [78] T. Abe, R. Sato and K. Yagyu, *Lepton-specific two Higgs doublet model as a solution of muon $g - 2$ anomaly*, *JHEP* **07** (2015) 064, [[1504.07059](#)].
- [79] E. J. Chun, S. Dwivedi, T. Mondal and B. Mukhopadhyaya, *Reconstructing a light pseudoscalar in the Type-X Two Higgs Doublet Model*, *Phys. Lett. B* **774** (2017) 20–25, [[1707.07928](#)].
- [80] E. J. Chun and J. Kim, *Leptonic Precision Test of Leptophilic Two-Higgs-Doublet Model*, *JHEP* **07** (2016) 110, [[1605.06298](#)].
- [81] A. Cherkhiglia, D. Stöckinger and H. Stöckinger-Kim, *Muon $g-2$ in the 2HDM: maximum results and detailed phenomenology*, *Phys. Rev. D* **98** (2018) 035001, [[1711.11567](#)].
- [82] L. Wang, J. M. Yang, M. Zhang and Y. Zhang, *Revisiting lepton-specific 2HDM in light of muon $g - 2$ anomaly*, *Phys. Lett. B* **788** (2019) 519–529, [[1809.05857](#)].
- [83] CMS collaboration, A. M. Sirunyan et al., *Search for a standard model-like Higgs boson in the mass range between 70 and 110 GeV in the diphoton final state in proton-proton collisions at $\sqrt{s} = 8$ and 13 TeV*, *Phys. Lett. B* **793** (2019) 320–347, [[1811.08459](#)].
- [84] S. M. Barr and A. Zee, *Electric Dipole Moment of the Electron and of the Neutron*, *Phys. Rev. Lett.* **65** (1990) 21–24.
- [85] V. Ilisie, *New Barr-Zee contributions to $(g - 2)_\mu$ in two-Higgs-doublet models*, *JHEP* **04** (2015) 077, [[1502.04199](#)].
- [86] R. H. Parker, C. Yu, W. Zhong, B. Estey and H. Müller, *Measurement of the fine-structure constant as a test of the Standard Model*, *Science* **360** (2018) 191, [[1812.04130](#)].
- [87] L. Morel, Z. Yao, P. Cladé and S. Guellati-Khélifa, *Determination of the fine-structure constant with an accuracy of 81 parts per trillion*, *Nature* **588** (2020) 61–65.
- [88] HFLAV collaboration, Y. S. Amhis et al., *Averages of b -hadron, c -hadron, and τ -lepton properties as of 2018*, *Eur. Phys. J. C* **81** (2021) 226, [[1909.12524](#)].
- [89] ALEPH collaboration, A. Heister et al., *Measurement of the Michel parameters and the ν /tau helicity in tau lepton decays*, *Eur. Phys. J. C* **22** (2001) 217–230.
- [90] G. C. Branco, P. M. Ferreira, L. Lavoura, M. N. Rebelo, M. Sher and J. P. Silva, *Theory and phenomenology of two-Higgs-doublet models*, *Phys. Rept.* **516** (2012) 1–102, [[1106.0034](#)].
- [91] S. L. Glashow and S. Weinberg, *Natural Conservation Laws for Neutral Currents*, *Phys. Rev. D* **15** (1977) 1958.
- [92] E. A. Paschos, *Diagonal Neutral Currents*, *Phys. Rev. D* **15** (1977) 1966.
- [93] M. Aoki, S. Kanemura, K. Tsumura and K. Yagyu, *Models of Yukawa interaction in the two Higgs doublet model, and their collider phenomenology*, *Phys. Rev. D* **80** (2009) 015017,

[0902.4665].

- [94] J. Song and Y. W. Yoon, *$W\gamma$ decay of the elusive charged Higgs boson in the two-Higgs-doublet model with vectorlike fermions*, *Phys. Rev. D* **100** (2019) 055006, [1904.06521].
- [95] ATLAS collaboration, *A combination of measurements of Higgs boson production and decay using up to 139 fb^{-1} of proton-proton collision data at $\sqrt{s} = 13\text{ TeV}$ collected with the ATLAS experiment*, .
- [96] M. Carena, I. Low, N. R. Shah and C. E. M. Wagner, *Impersonating the Standard Model Higgs Boson: Alignment without Decoupling*, *JHEP* **04** (2014) 015, [1310.2248].
- [97] A. Celis, V. Ilisie and A. Pich, *LHC constraints on two-Higgs doublet models*, *JHEP* **07** (2013) 053, [1302.4022].
- [98] J. Bernon, J. F. Gunion, H. E. Haber, Y. Jiang and S. Kraml, *Scrutinizing the alignment limit in two-Higgs-doublet models: $m_h=125\text{ GeV}$* , *Phys. Rev. D* **92** (2015) 075004, [1507.00933].
- [99] S. Chang, S. K. Kang, J.-P. Lee and J. Song, *Higgs potential and hidden light Higgs scenario in two Higgs doublet models*, *Phys. Rev. D* **92** (2015) 075023, [1507.03618].
- [100] D. Das and I. Saha, *Search for a stable alignment limit in two-Higgs-doublet models*, *Phys. Rev. D* **91** (2015) 095024, [1503.02135].
- [101] J. Bernon, J. F. Gunion, H. E. Haber, Y. Jiang and S. Kraml, *Scrutinizing the alignment limit in two-Higgs-doublet models. II. $m_H=125\text{ GeV}$* , *Phys. Rev. D* **93** (2016) 035027, [1511.03682].
- [102] ATLAS collaboration, G. Aad et al., *Combined measurements of Higgs boson production and decay using up to 80 fb^{-1} of proton-proton collision data at $\sqrt{s} = 13\text{ TeV}$ collected with the ATLAS experiment*, *Phys. Rev. D* **101** (2020) 012002, [1909.02845].
- [103] I. P. Ivanov, *Minkowski space structure of the Higgs potential in 2HDM*, *Phys. Rev. D* **75** (2007) 035001, [hep-ph/0609018].
- [104] A. Barroso, P. M. Ferreira, I. P. Ivanov and R. Santos, *Metastability bounds on the two Higgs doublet model*, *JHEP* **06** (2013) 045, [1303.5098].
- [105] A. Arhrib, *Unitarity constraints on scalar parameters of the standard and two Higgs doublets model*, in *Workshop on Noncommutative Geometry, Superstrings and Particle Physics*, 12, 2000. hep-ph/0012353.
- [106] M. E. Peskin and T. Takeuchi, *Estimation of oblique electroweak corrections*, *Phys. Rev. D* **46** (1992) 381–409.
- [107] PARTICLE DATA GROUP collaboration, P. A. Zyla et al., *Review of Particle Physics*, *PTEP* **2020** (2020) 083C01.
- [108] H.-J. He, N. Polonsky and S.-f. Su, *Extra families, Higgs spectrum and oblique corrections*, *Phys. Rev. D* **64** (2001) 053004, [hep-ph/0102144].
- [109] W. Grimus, L. Lavoura, O. M. Ogreid and P. Osland, *The Oblique parameters in multi-Higgs-doublet models*, *Nucl. Phys. B* **801** (2008) 81–96, [0802.4353].
- [110] P. Bechtle, S. Heinemeyer, O. Stål, T. Stefaniak and G. Weiglein, *HiggsSignals: Confronting arbitrary Higgs sectors with measurements at the Tevatron and the LHC*, *Eur. Phys. J. C* **74** (2014) 2711, [1305.1933].

- [111] P. Bechtle, S. Heinemeyer, T. Klingl, T. Stefaniak, G. Weiglein and J. Wittbrodt, *HiggsSignals-2: Probing new physics with precision Higgs measurements in the LHC 13 TeV era*, *Eur. Phys. J. C* **81** (2021) 145, [2012.09197].
- [112] P. Bechtle, D. Dercks, S. Heinemeyer, T. Klingl, T. Stefaniak, G. Weiglein et al., *HiggsBounds-5: Testing Higgs Sectors in the LHC 13 TeV Era*, *Eur. Phys. J. C* **80** (2020) 1211, [2006.06007].
- [113] ALEPH, DELPHI, L3, OPAL, LEP WORKING GROUP FOR HIGGS BOSON SEARCHES collaboration, S. Schael et al., *Search for neutral MSSM Higgs bosons at LEP*, *Eur. Phys. J. C* **47** (2006) 547–587, [hep-ex/0602042].
- [114] ATLAS collaboration, M. Aaboud et al., *Search for Higgs boson decays into a pair of light bosons in the $b\bar{b}\mu\mu$ final state in pp collision at $\sqrt{s}=13$ TeV with the ATLAS detector*, *Phys. Lett. B* **790** (2019) 1–21, [1807.00539].
- [115] ATLAS collaboration, M. Aaboud et al., *Search for the Higgs boson produced in association with a vector boson and decaying into two spin-zero particles in the $H \rightarrow aa \rightarrow 4b$ channel in pp collisions at $\sqrt{s}=13$ TeV with the ATLAS detector*, *JHEP* **10** (2018) 031, [1806.07355].
- [116] CMS collaboration, A. M. Sirunyan et al., *Search for an exotic decay of the Higgs boson to a pair of light pseudoscalars in the final state of two muons and two τ leptons in proton-proton collisions at $\sqrt{s}=13$ TeV*, *JHEP* **11** (2018) 018, [1805.04865].
- [117] CMS collaboration, A. M. Sirunyan et al., *Search for an exotic decay of the Higgs boson to a pair of light pseudoscalars in the final state with two muons and two b quarks in pp collisions at 13 TeV*, *Phys. Lett. B* **795** (2019) 398–423, [1812.06359].
- [118] CMS collaboration, A. M. Sirunyan et al., *Search for an exotic decay of the Higgs boson to a pair of light pseudoscalars in the final state with two b quarks and two τ leptons in proton-proton collisions at $\sqrt{s}=13$ TeV*, *Phys. Lett. B* **785** (2018) 462, [1805.10191].
- [119] CMS collaboration, A. M. Sirunyan et al., *Search for light pseudoscalar boson pairs produced from decays of the 125 GeV Higgs boson in final states with two muons and two nearby tracks in pp collisions at $\sqrt{s}=13$ TeV*, *Phys. Lett. B* **800** (2020) 135087, [1907.07235].
- [120] ATLAS collaboration, M. Aaboud et al., *Combination of searches for heavy resonances decaying into bosonic and leptonic final states using 36 fb^{-1} of proton-proton collision data at $\sqrt{s}=13$ TeV with the ATLAS detector*, *Phys. Rev. D* **98** (2018) 052008, [1808.02380].
- [121] CMS collaboration, A. M. Sirunyan et al., *Search for a new scalar resonance decaying to a pair of Z bosons in proton-proton collisions at $\sqrt{s}=13$ TeV*, *JHEP* **06** (2018) 127, [1804.01939].
- [122] CMS collaboration, A. M. Sirunyan et al., *Search for a heavy Higgs boson decaying to a pair of W bosons in proton-proton collisions at $\sqrt{s}=13$ TeV*, *JHEP* **03** (2020) 034, [1912.01594].
- [123] CMS collaboration, A. M. Sirunyan et al., *Combination of searches for Higgs boson pair production in proton-proton collisions at $\sqrt{s}=13$ TeV*, *Phys. Rev. Lett.* **122** (2019) 121803, [1811.09689].
- [124] ATLAS collaboration, M. Aaboud et al., *Search for Higgs boson pair production in the $\gamma\gamma WW^*$ channel using pp collision data recorded at $\sqrt{s}=13$ TeV with the ATLAS detector*, *Eur. Phys. J. C* **78** (2018) 1007, [1807.08567].

- [125] ATLAS collaboration, M. Aaboud et al., *Search for pair production of Higgs bosons in the $b\bar{b}b\bar{b}$ final state using proton-proton collisions at $\sqrt{s} = 13$ TeV with the ATLAS detector*, *JHEP* **01** (2019) 030, [[1804.06174](#)].
- [126] ATLAS collaboration, M. Aaboud et al., *Search for Higgs boson pair production in the $WW^{(*)}WW^{(*)}$ decay channel using ATLAS data recorded at $\sqrt{s} = 13$ TeV*, *JHEP* **05** (2019) 124, [[1811.11028](#)].
- [127] ATLAS collaboration, M. Aaboud et al., *Search for resonant and non-resonant Higgs boson pair production in the $b\bar{b}\tau^+\tau^-$ decay channel in pp collisions at $\sqrt{s} = 13$ TeV with the ATLAS detector*, *Phys. Rev. Lett.* **121** (2018) 191801, [[1808.00336](#)].
- [128] ATLAS collaboration, G. Aad et al., *Combination of searches for Higgs boson pairs in pp collisions at $\sqrt{s} = 13$ TeV with the ATLAS detector*, *Phys. Lett. B* **800** (2020) 135103, [[1906.02025](#)].
- [129] ATLAS collaboration, G. Aad et al., *Search for the $HH \rightarrow b\bar{b}b\bar{b}$ process via vector-boson fusion production using proton-proton collisions at $\sqrt{s} = 13$ TeV with the ATLAS detector*, *JHEP* **07** (2020) 108, [[2001.05178](#)].
- [130] ATLAS collaboration, M. Aaboud et al., *Search for new phenomena in high-mass diphoton final states using 37 fb^{-1} of proton-proton collisions collected at $\sqrt{s} = 13$ TeV with the ATLAS detector*, *Phys. Lett. B* **775** (2017) 105–125, [[1707.04147](#)].
- [131] CMS collaboration, A. M. Sirunyan et al., *Search for a standard model-like Higgs boson in the mass range between 70 and 110 GeV in the diphoton final state in proton-proton collisions at $\sqrt{s} = 8$ and 13 TeV*, *Phys. Lett. B* **793** (2019) 320–347, [[1811.08459](#)].
- [132] CMS collaboration, A. M. Sirunyan et al., *Search for additional neutral MSSM Higgs bosons in the $\tau\tau$ final state in proton-proton collisions at $\sqrt{s} = 13$ TeV*, *JHEP* **09** (2018) 007, [[1803.06553](#)].
- [133] ATLAS collaboration, G. Aad et al., *Search for heavy Higgs bosons decaying into two tau leptons with the ATLAS detector using pp collisions at $\sqrt{s} = 13$ TeV*, *Phys. Rev. Lett.* **125** (2020) 051801, [[2002.12223](#)].
- [134] ATLAS collaboration, G. Aad et al., *Search for high-mass dilepton resonances using 139 fb^{-1} of pp collision data collected at $\sqrt{s} = 13$ TeV with the ATLAS detector*, *Phys. Lett. B* **796** (2019) 68–87, [[1903.06248](#)].
- [135] ATLAS collaboration, M. Aaboud et al., *Search for scalar resonances decaying into $\mu^+\mu^-$ in events with and without b-tagged jets produced in proton-proton collisions at $\sqrt{s} = 13$ TeV with the ATLAS detector*, *JHEP* **07** (2019) 117, [[1901.08144](#)].
- [136] CMS collaboration, A. M. Sirunyan et al., *Search for MSSM Higgs bosons decaying to $\mu + \mu -$ in proton-proton collisions at $s=13\text{TeV}$* , *Phys. Lett. B* **798** (2019) 134992, [[1907.03152](#)].
- [137] CMS collaboration, A. M. Sirunyan et al., *Search for low-mass resonances decaying into bottom quark-antiquark pairs in proton-proton collisions at $\sqrt{s} = 13$ TeV*, *Phys. Rev. D* **99** (2019) 012005, [[1810.11822](#)].
- [138] CMS collaboration, A. M. Sirunyan et al., *Search for beyond the standard model Higgs bosons decaying into a $b\bar{b}$ pair in pp collisions at $\sqrt{s} = 13$ TeV*, *JHEP* **08** (2018) 113, [[1805.12191](#)].

- [139] ATLAS collaboration, G. Aad et al., *Search for heavy neutral Higgs bosons produced in association with b-quarks and decaying into b-quarks at $\sqrt{s} = 13$ TeV with the ATLAS detector*, *Phys. Rev. D* **102** (2020) 032004, [[1907.02749](#)].
- [140] CMS collaboration, A. M. Sirunyan et al., *Search for heavy Higgs bosons decaying to a top quark pair in proton-proton collisions at $\sqrt{s} = 13$ TeV*, *JHEP* **04** (2020) 171, [[1908.01115](#)].
- [141] ATLAS collaboration, G. Aad et al., *Search for a CP-odd Higgs boson decaying to Zh in pp collisions at $\sqrt{s} = 8$ TeV with the ATLAS detector*, *Phys. Lett. B* **744** (2015) 163–183, [[1502.04478](#)].
- [142] CMS collaboration, A. M. Sirunyan et al., *Search for a heavy pseudoscalar boson decaying to a Z and a Higgs boson at $\sqrt{s} = 13$ TeV*, *Eur. Phys. J. C* **79** (2019) 564, [[1903.00941](#)].
- [143] ATLAS collaboration, M. Aaboud et al., *Search for a heavy Higgs boson decaying into a Z boson and another heavy Higgs boson in the $\ell\ell b\bar{b}$ final state in pp collisions at $\sqrt{s} = 13$ TeV with the ATLAS detector*, *Phys. Lett. B* **783** (2018) 392–414, [[1804.01126](#)].
- [144] CMS collaboration, A. M. Sirunyan et al., *Search for new neutral Higgs bosons through the $H \rightarrow ZA \rightarrow \ell^+ \ell^- b\bar{b}$ process in pp collisions at $\sqrt{s} = 13$ TeV*, *JHEP* **03** (2020) 055, [[1911.03781](#)].
- [145] ATLAS collaboration, M. Aaboud et al., *Search for charged Higgs bosons decaying into top and bottom quarks at $\sqrt{s} = 13$ TeV with the ATLAS detector*, *JHEP* **11** (2018) 085, [[1808.03599](#)].
- [146] CMS collaboration, A. M. Sirunyan et al., *Search for charged Higgs bosons decaying into a top and a bottom quark in the all-jet final state of pp collisions at $\sqrt{s} = 13$ TeV*, *JHEP* **07** (2020) 126, [[2001.07763](#)].
- [147] ATLAS collaboration, M. Aaboud et al., *Search for charged Higgs bosons decaying via $H^\pm \rightarrow \tau^\pm \nu_\tau$ in the τ +jets and τ +lepton final states with 36 fb $^{-1}$ of pp collision data recorded at $\sqrt{s} = 13$ TeV with the ATLAS experiment*, *JHEP* **09** (2018) 139, [[1807.07915](#)].
- [148] CMS collaboration, A. M. Sirunyan et al., *Search for charged Higgs bosons in the $H^\pm \rightarrow \tau^\pm \nu_\tau$ decay channel in proton-proton collisions at $\sqrt{s} = 13$ TeV*, *JHEP* **07** (2019) 142, [[1903.04560](#)].
- [149] CMS collaboration, V. Khachatryan et al., *Search for light bosons in decays of the 125 GeV Higgs boson in proton-proton collisions at $\sqrt{s} = 8$ TeV*, *JHEP* **10** (2017) 076, [[1701.02032](#)].
- [150] ALEPH, DELPHI, L3, OPAL, LEP collaboration, G. Abbiendi et al., *Search for Charged Higgs bosons: Combined Results Using LEP Data*, *Eur. Phys. J. C* **73** (2013) 2463, [[1301.6065](#)].
- [151] T. Aoyama, T. Kinoshita and M. Nio, *Revised and Improved Value of the QED Tenth-Order Electron Anomalous Magnetic Moment*, *Phys. Rev. D* **97** (2018) 036001, [[1712.06060](#)].
- [152] S. Laporta, *High-precision calculation of the 4-loop contribution to the electron g-2 in QED*, *Phys. Lett. B* **772** (2017) 232–238, [[1704.06996](#)].
- [153] M. Grazzini, S. Kallweit and D. Rathlev, *ZZ production at the LHC: fiducial cross sections and distributions in NNLO QCD*, *Phys. Lett. B* **750** (2015) 407–410, [[1507.06257](#)].
- [154] ATLAS collaboration, G. Aad et al., *Measurement of the ZZ Production Cross Section in pp Collisions at $\sqrt{s} = 13$ TeV with the ATLAS Detector*, *Phys. Rev. Lett.* **116** (2016) 101801, [[1512.05314](#)].
- [155] ATLAS collaboration, M. Aaboud et al., *Measurement of fiducial and differential W^+W^- production cross-sections at $\sqrt{s} = 13$ TeV with the ATLAS detector*, *Eur. Phys. J. C* **79** (2019)

884, [[1905.04242](#)].

- [156] L. Michel, *Interaction between four half spin particles and the decay of the μ meson*, *Proc. Phys. Soc. A* **63** (1950) 514–531.
- [157] H. E. Logan and D. MacLennan, *Charged Higgs phenomenology in the lepton-specific two Higgs doublet model*, *Phys. Rev. D* **79** (2009) 115022, [[0903.2246](#)].
- [158] A. Stahl, *Michel parameters: Averages and interpretation*, *Nucl. Phys. B Proc. Suppl.* **76** (1999) 173–181.
- [159] BELLE collaboration, N. Shimizu et al., *Measurement of the tau Michel parameters $\bar{\eta}$ and $\xi\kappa$ in the radiative leptonic decay $\tau^- \rightarrow \ell^- \nu_\tau \bar{\nu}_\ell \gamma$* , *PTEP* **2018** (2018) 023C01, [[1709.08833](#)].
- [160] S. Gentile and M. Pohl, *Physics of τ leptons*, *Phys. Rept.* **274** (1996) 287–376.
- [161] ALEPH, DELPHI, L3, OPAL, SLD, LEP ELECTROWEAK WORKING GROUP, SLD ELECTROWEAK GROUP, SLD HEAVY FLAVOUR GROUP collaboration, S. Schael et al., *Precision electroweak measurements on the Z resonance*, *Phys. Rept.* **427** (2006) 257–454, [[hep-ex/0509008](#)].